Marine Micropaleontology 92–93 (2012) 61–80

Contents lists available at SciVerse ScienceDirect

Marine Micropaleontology

journal homepage: www.elsevier.com/locate/marmicro

Calcareous nannofossil assemblage changes across the Paleocene–Eocene Thermal Maximum: Evidence from a shelf setting

Jean M. Self-Trail [a,*], David S. Powars [a], David K. Watkins [b], Gregory A. Wandless [c]

[a] U.S. Geological Survey, 926a National Center, Reston, VA 20192, USA
[b] Department of Earth and Atmospheric Sciences, University of Nebraska, Lincoln, NE, USA
[c] U.S. Geological Survey, 951 National Center, Reston, VA 20192, USA

ARTICLE INFO

Article history:
Received 15 November 2011
Received in revised form 14 March 2012
Accepted 12 May 2012
Available online 18 May 2012

Keywords:
Paleocene–Eocene Thermal Maximum
calcareous nannofossils
paleoclimate

ABSTRACT

Biotic response of calcareous nannoplankton to abrupt warming across the Paleocene/Eocene boundary reflects a primary response to climatically induced parameters including increased continental runoff of freshwater, global acidification of seawater, high sedimentation rates, and calcareous nannoplankton assemblage turnover. We identify ecophenotypic nannofossil species adapted to low pH conditions (*Discoaster anartios, D. araneus, Rhomboaster* spp.), excursion taxa adapted to the extremely warm climatic conditions (*Bomolithus supremus* and *Coccolithus bownii*), three species of the genus *Toweius* (*T. serotinus, T. callosus, T. occultatus*) adapted to warm, rather than cool, water conditions, opportunists adapted to high productivity conditions (*Coronocyclus bramlettei, Neochiastozygus junctus*), and species adapted to oligotropic and/or cool-water conditions that went into refugium during the PETM (*Zygrablithus bijugatus, Calcidiscus? parvicrucis* and *Chiasmolithus bidens*). *Discoaster anartios* was adapted to meso- to eutrophic, rather than oligotrophic, conditions. Comparison of these data to previous work on sediments deposited on shelf settings suggests that local conditions such as high precipitation rates and possible increase in major storms such as hurricanes resulted in increased continental runoff and high sedimentation rates that affected assemblage response to the PETM.

Published by Elsevier B.V.

1. Introduction

The Paleocene/Eocene Thermal Maximum (PETM) represents a time of extreme global greenhouse warmth whose rapid onset (under 10,000 years) occurred at approximately 55.33 Ma and lasted for ~170 kyr (Rohl et al., 2007). Deep-ocean drilling data suggest that sea-surface temperatures increased in northern high latitudes by 10–12 °C, by 8 °C in southern high latitudes, and by about 4–5 °C in equatorial settings. Mid-latitude continental interior temperatures are thought to have increased by about 5 °C (Thomas et al., 2006). Global atmospheric temperatures are thought to have risen between 5 and 9 °C (Kennett and Stott, 1991; Zachos et al., 2003; Sluijs et al., 2006). An accompanying negative carbon isotope ($\delta^{13}C$) excursion (CIE) is documented from both marine and terrestrial sediments.

First identified from ODP Sites 689 and 690 (Kennett and Stott, 1990, 1991), the CIE has subsequently been used to delineate the Paleocene/Eocene boundary worldwide (Aubry and Ouda, 2003). Associated with this event is a benthic foraminiferal extinction event in deep-sea records, a turnover in mammalian fauna in terrestrial records, and the appearance of excursion taxa in both planktic foraminifera and calcareous nannofossils. Changes in the biotic realm are a reflection of rapid and extreme paleoceanographic changes that point to a greenhouse world characterized by increased temperature and precipitation.

Biotic response to this rapid and extreme warming event has been documented from a number of locales using a variety of organisms, including marine and terrestrial palynomorphs, planktic and benthic foraminifers, and calcareous nannoplankton. The biotic response of calcareous nannofossils to the PETM has been documented from a variety of deep-ocean settings, including Site 690 in the Southern Ocean (Bralower, 2002; Angori et al., 2007), Site 527 in the Southern Atlantic (Kahn and Aubry, 2004), Sites 1260B and 1259B from the Equatorial Atlantic (Jiang and Wise, 2006; Mutterlose et al., 2007), Site 401 in the North Atlantic (Tremolada and Bralower, 2004); Sites 1209, 1215, 1220, and 1221 from the Equatorial Pacific (Raffi et al., 2005; Gibbs et al., 2006a); and Site 213 from the Indian Ocean (Tremolada and Bralower, 2004), among others. Additionally, a number of Tethyan Seaway sites have been documented from Egypt, Spain and Italy (Agnini et al., 2007; Angori et al., 2007), and an exceptionally well-preserved section has been documented from an expanded section in southern Tanzania (Bown et al., 2008; Bown and Pearson, 2009). Paleodepths in the Tethyan sections are typically shallower than the deep-ocean sites, attaining average depths between 1000 and 2000 m, with the Wadi Nukhl section in Egypt being the shallowest

* Corresponding author. Tel.: +1 703 648 6013; fax: +1 703 648 6953.
E-mail address: jstrail@usgs.gov (J.M. Self-Trail).

0377-8398/$ – see front matter. Published by Elsevier B.V.
doi:10.1016/j.marmicro.2012.05.003

at ~500 m (Speijer et al., 2000; Angori et al., 2007). The Tanzanian section was deposited in a bathyal to outer shelf environment at water depths of 300–500 m.

Relatively few shallow marine sections spanning the Paleocene/Eocene (P/E) boundary have been identified or studied for calcareous nannofossil content. In part, this is due to the paucity of available cores. In the New Jersey coastal plain of the eastern United States, several P/E boundary sites (Bass River, Clayton, and Wilson Lake cores) have been identified and analyzed for calcareous nannofossil and geochemical content (Bybell and Self-Trail, 1995; Kahn and Aubry, 2004; Gibbs et al., 2006a). Sediments at these sites were most likely deposited in middle to outer neritic water depths (30–180 m; Kopp et al., 2009; Sluijs and Brinkhuis, 2009). Recent drilling by the U.S. Geological Survey on the eastern shore of Maryland (Fig. 1) recovered a nearly continuous PETM section (16.9 m) that contains an exceptionally rich and well-preserved calcareous nannofossil flora (Self-Trail, 2011). Analysis of planktic/benthic (P/B) foraminifera ratios, dinoflagellate abundances, and sedimentology suggests that sediments were most likely deposited in a middle neritic setting, with estimated water depths of 30–100 m, making this the shallowest known marine PETM section to be analyzed for calcareous nannofossil content.

The goal of this paper is to examine abundance fluctuations of selected calcareous nannofossil taxa from the South Dover Bridge (SDB) core and compare them with assemblage data from other nearby shelf locations (e.g., Wilson Lake and Bass River) with the purpose of: (1) identifying a calcareous nannofossil excursion assemblage restricted to the PETM of this region, (2) documenting the changeover in floral assemblages from those representative of cool and/or eutrophic conditions to those representative of warm and/or oligotrophic conditions, and (3) combining biostratigraphic data with lithologic interpretations in an effort to determine the role that freshwater river influx, sedimentation, and nutrients played in controlling calcareous nannofossil populations.

2. Geologic setting

The SDB core is situated near the central axis of the Salisbury Embayment of the mid-Atlantic Coastal Plain, a deep basement trough

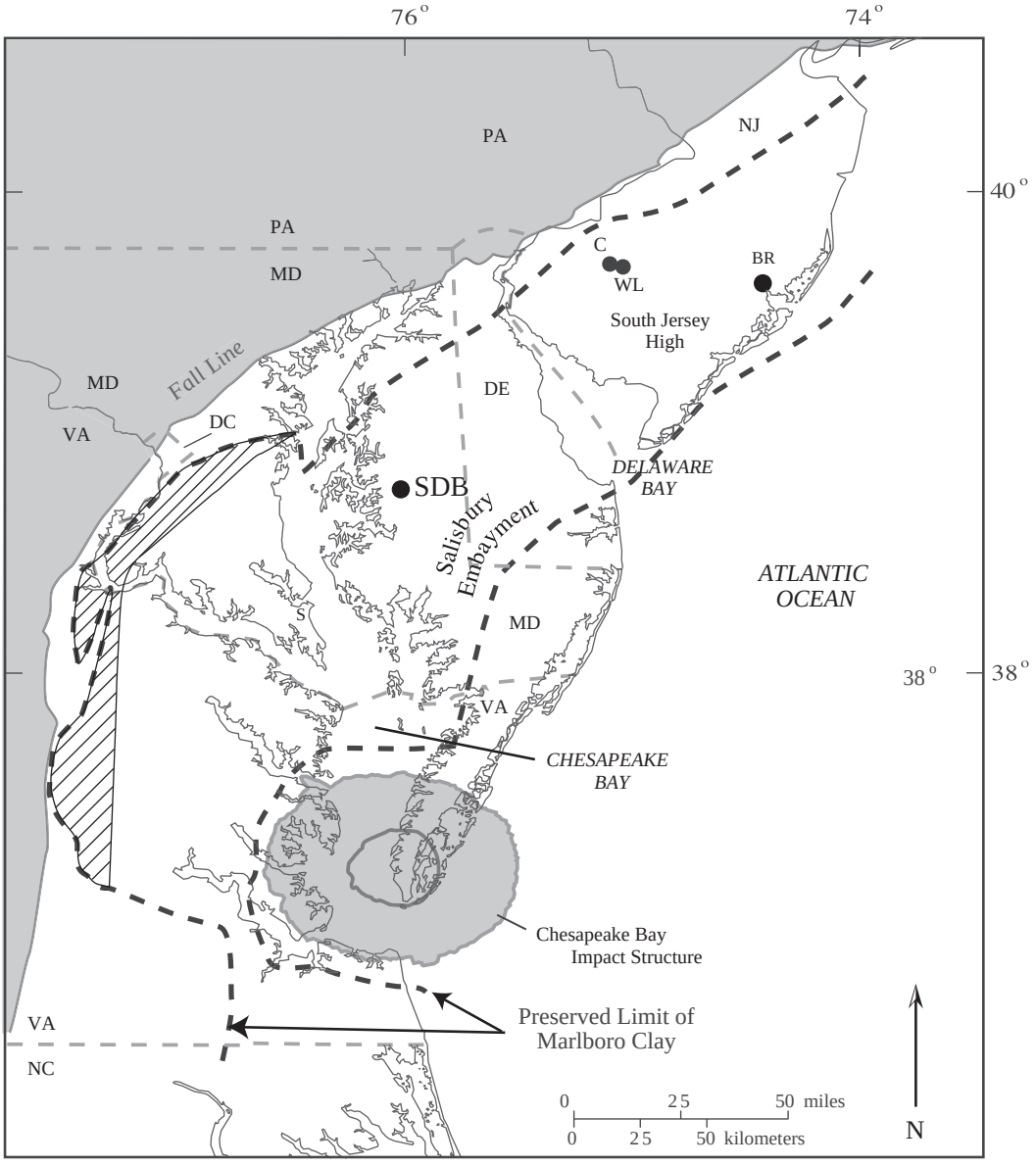

Fig. 1. Map showing the location of coreholes (dots) discussed in the text. SDB (South Dover Bridge); BR (Bass River); WL (Wilson Lake); C (Clayton). Hatchured section shows the outcrop area of the Marlboro Clay and black dashed lines indicate the preserved extent, both subsurface and subaerial, of the Marlboro Clay.

bounded to the north by the South Jersey High and to the south by the Norfolk Arch (Gibson and Bybell, 1994a; Kopp et al., 2009). It is located at 38°44′49″N latitude and 76°00′25″W longitude in Talbot County, Maryland (Fig. 1), with a surface altitude of 3.6 m. A total depth of 214.6 m was attained during coring. The exact paleolatitude of the Salisbury Embayment during the late Paleocene and early Eocene is difficult to determine. Kopp et al. (2007) suggest a paleolatitude of 25–28°N based on data from the Faroe-Rockall Plateau, and a more northerly paleolatitude of 35–40°N was calculated by Muller et al. (2008) based on reconstruction of seafloor isochrons. These data sets suggest that this site was located in a subtropical to temperate paleolatitude during deposition, and thus was probably subject to seasonal cold and warm-water influence.

The Paleocene/Eocene boundary sequence comprises three depositional units restricted to the Salisbury Basin: the Aquia Formation (upper Paleocene), the Marlboro Clay (lower Eocene), and the Nanjemoy Formation (lower Eocene). Regionally, the Aquia Formation consists of a black to greenish-black to dark and light greenish-gray, massive to thinly stratified, clayey and silty, very fine to coarse glauconitic (20–75%) quartz sand, with variable amounts of shells, microfossils, burrows, mica, pyrite, lignitic material, and calcium carbonate cemented layers and concretions (Hansen, 1974; Reinhardt et al., 1980; Mixon et al., 1989; Gibson and Bybell, 1994b; Powars and Bruce, 1999). Based on benthic and planktic foraminiferal assemblage data, the Aquia Formation is thought to represent inner neritic to middle neritic environments deposited in paleodepths less than 40–50 m (Gibson and Bybell, 1994a). The Aquia/Marlboro contact in most outcrops and cores is a highly burrowed sharp unconformity that can be traced across the basin (Gibson et al., 2000; Kopp et al., 2009).

The Marlboro Clay has been mapped across the mid-Atlantic Coastal Plain from northern New Jersey to the eastern Virginia–North Carolina border. It is a relatively thin unit that ranges from a feathers edge updip to 15.6 m in the SDB core (Fig. 2). The unit is thinnest on the uplifted sides of faults due to truncation and syndepositional thinning (Mixon and Powars, 1984; Powars and Bruce,

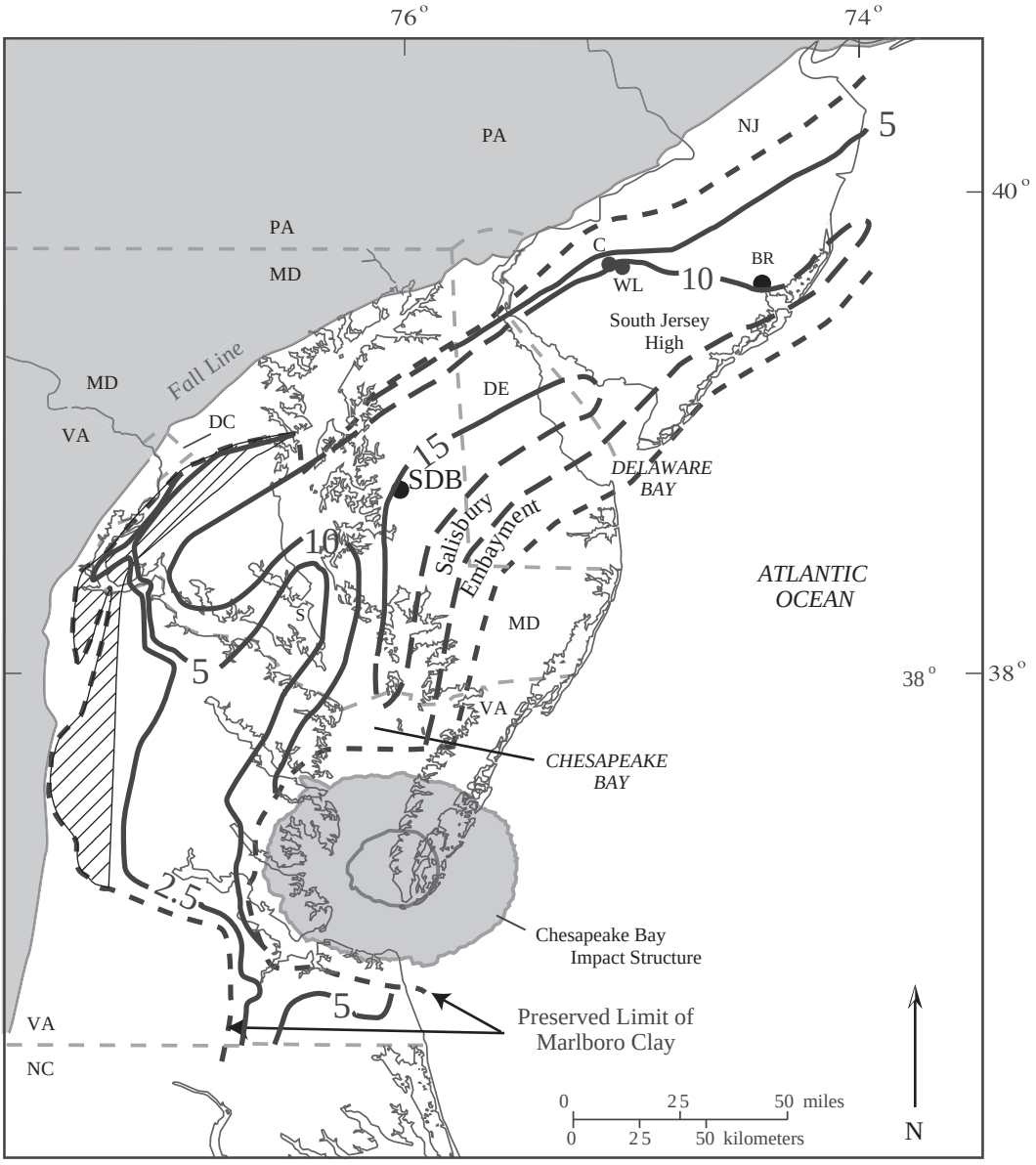

Fig. 2. Isopach map of the Marlboro Clay across the mid-Atlantic region, with thicknesses in meters. Solid lines indicate known thickness; dashed lines inferred where data are lacking. Dots indicate location of coreholes discussed in text. SDB (South Dover Bridge); BR (Bass River); WL (Wilson Lake); C (Clayton). Hatchured section shows the outcrop area of the Marlboro Clay.
Modified from Kopp et al. (2009)

1999; Powars, pers. comm.) and thickens on the down-dropped sides of faults which acted as sinks and were not subject to erosion. The Marlboro Clay typically consists of light-gray to pinkish-gray to reddish-brown, massive, kaolinite-dominated clayey silt to silty clay with occasional to abundant light-gray to very pale brown to pale yellow to white, thin beds, laminations, and discontinuous wisps of silt. Some of these silt layers include very fine quartz sand. Previous investigations recorded the presence of benthic and planktic foraminifers representative of inner to middle neritic water depths and low diversity calcareous nannofossil assemblages indicative of partially restricted to open-ocean circulation (Gibson and Bybell, 1994b; Kopp et al., 2009).

The Nanjemoy Formation is lithologically similar to the Aquia Formation and typically consists of dark-olive-gray to greenish-gray to olive-black, massive to thinly bedded, variably clayey, silty, fine to coarse glauconitic (15–85%) quartz sand with varying amounts of shells, microfossils, mica, lignitic material, pyrite, and calcium carbonate cemeted layers and nodules (Mixon et al., 1989; Powars and Bruce, 1999). It is characteristically intensely burrowed (Mixon et al., 1989; Gibson and Bybell, 1994a; Powars and Bruce, 1999). This unit generally contains several fining-upward sequences that are often truncated in updip and structurally uplifted areas (Mixon et al., 1989; Powars and Bruce, 1999). Calcareous nannofossil data indicate an early Eocene age (Zones NP 10 through NP14), and foraminiferal data from the Solomons Island and Putney Mills cores suggest that the lowest part of the Nanjemoy was deposited in inner neritic environments of less than 30 m, grading up into inner to middle neritic water depths varying from 60 m to 300 m (Bybell and Gibson, 1994; Gibson and Bybell, 1994b). Poag (1989) reported water depths of 20–150 m for the Nanjemoy of the Haynesville core based on foraminifera analyses.

In the SDB core, the Aquia consists of greenish-black to dark-yellowish-green to dark-greenish-gray, variably clayey, silty to fairly clean very fine to medium glauconitic (25–90%) quartz sand, with scattered coarse to very coarse angular to rounded quartz grains, burrows, and microfossils. Silt to medium-sized mica flakes vary from scattered to abundant. The Marlboro/Aquia contact in the SDB core is placed at 204.0 m where the massive [grayish-olive-green with a tint of red] clayey silt overlies sharply, and is burrowed down into the greenish-black, very fine glauconite-rich quartz sand (Fig. 3). The basal 3 cm of Marlboro Clay includes a gradual increase downward of very fine glauconite (1–5%) to the sharp contact with the Aquia and is interpreted as reworked glauconite from the Aquia. The calcareous nannofossil assemblage data indicate this unconformity represents very little (<0.9 my) missing time (Self-Trail, 2011).

The Marlboro Clay is 15.6 m thick in the SDB core and consists of grayish-olive-green to dusky-olive-green massive to laminated to wispy clay to angular silt to clayey silt, with scattered very fine to fine angular quartz grains within some laminations, discontinuous

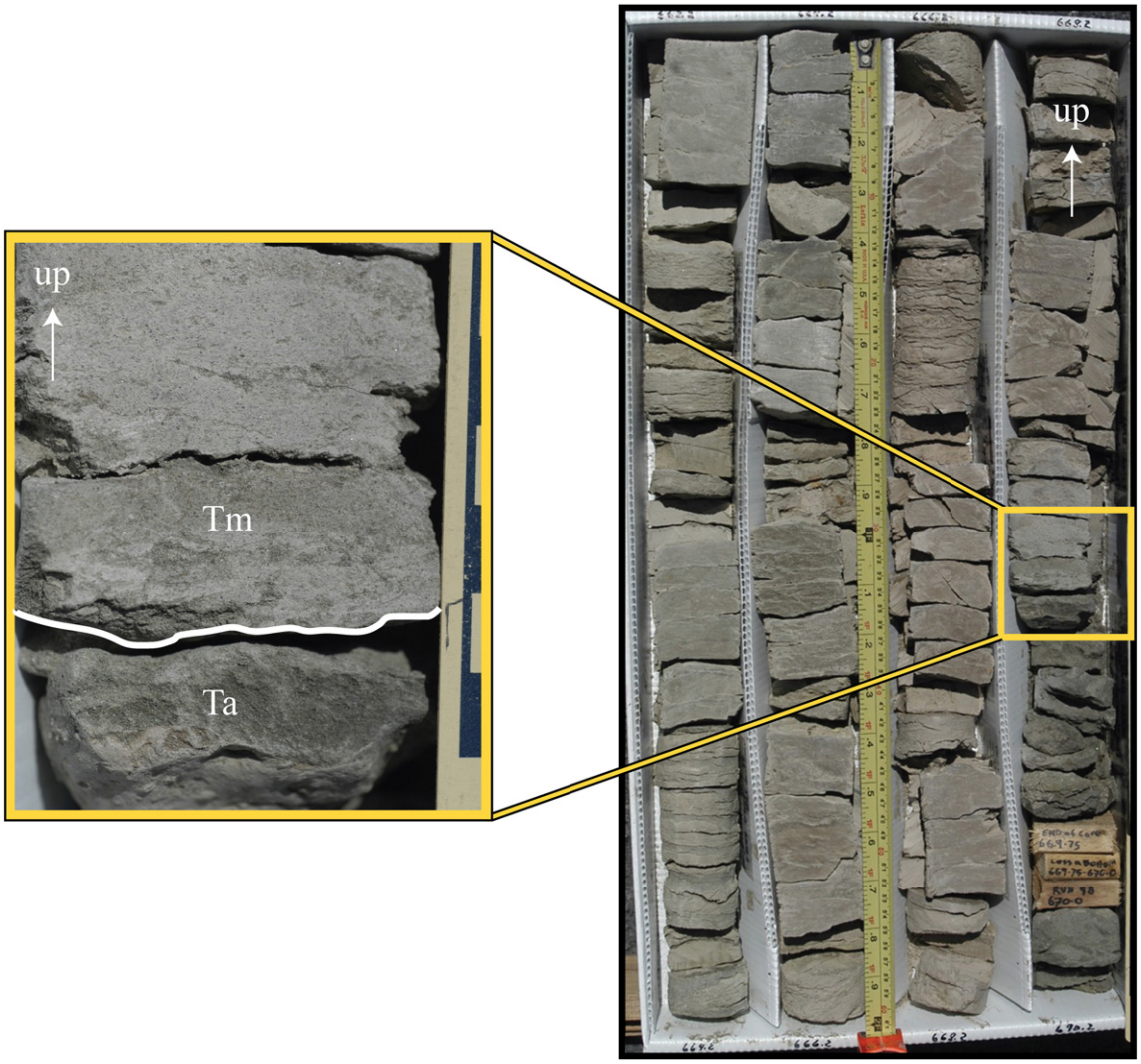

Fig. 3. Photograph of Box 73, from 201.8 m to 204.3 m, containing the Aquia Formation (Ta)/Marlboro Clay (Tm) contact in the South Dover Bridge core. Insert shows close-up of the contact (white line; 204.0 m). Arrows show stratigraphic up.

wisps, and concentrated in some burrows. Dark-green rounded silt to fine glauconite grains (1–7%) are present. There are scattered small to tiny wood fragments and small shell fragments and molds in the lower half of the unit. Wood and organic materials are oriented horizontally along bedding surfaces and pyrite nodules and fine-disseminated pyrite are scattered throughout. The contact between the gray silty clay of the Marlboro and the overlying black to greenish-black silty clayey very fine to medium glauconitic quartz sand of the Nanjemoy Formation is highly burrowed and is located at 188.4 m (Fig. 4), suggesting that some section is missing. However, although the calcareous nannofossil assemblage in the SDB core is more diverse than any previously recorded, there is no indication of missing time across the Marlboro/Nanjemoy boundary, and thus any missing section falls within one nannofossil zone. Frederiksen (1979) reported a fern spike at the base of the Marlboro in the Oak Grove core (Virginia) and Willard et al. (2009) reported a similar spike in the SDB core. The fern spike coupled with the dominance of kaolinite throughout the Marlboro Clay suggests a relatively moist climate with increased continental runoff at the time of deposition (Gibson et al., 2000; Kopp et al., 2009).

The basal Nanjemoy Formation, from 188.4 m to 187.05 m, represents a highly burrowed interval truncated by a disconformable contact at 187.05 m that marks the NP10/NP11 boundary (Fig. 4). Only 0.36 m of unrecovered core is recorded from the 2.35 m section cored between the disconformity at 187.05 m and the bottom of the figured section at 189.4 m, for an average 85% core recovery in this section (Fig. 4; Aleman pers. comm., 2012). The basal 0.6 m of the Nanjemoy Formation in the SDB core is a highly burrowed mixture of clayey silty very fine to medium glauconitic (75–80%) quartz sand with shell fragments and molds and very fine to fine glauconitic (15–30%) sandy silty clay with scattered very fine to medium quartz grains. Both lithologies contain up to 5% foraminifera, and the burrows are from 2 to 10 mm in diameter. A very fine pebble-sized reddish-gray rip-up clast of the Marlboro Clay is present. Shell fragments decrease in abundance upsection from the contact with the Marlboro Clay, where a few very fine phosphate and/or glauconite pebbles are present. The absence of *Rhomboaster contortus* and *R. digitalis* in this Zone NP10 material suggests that the upper part of Zone NP10 has been truncated by erosion and is missing in the SDB core (Self-Trail et al., 2010; Self-Trail, 2011) (Fig. 5). The base of the slightly glauconitic silty clay unit is at 187.05 m where it sharply overlies a clayey silty glauconitic (75%) quartz sand that represents the Zone NP10/NP11 disconformable boundary (Fig. 4). This contact is interpreted to represent the end of the PETM event.

3. Paleocene/Eocene boundary

Identification of the P/E boundary in the SDB core is based on an almost 3–4‰ negative shift in bulk $\delta^{13}C$ and the identification of calcareous nannofossil Zones NP9 and NP10. The beginning of the CIE is rapid and easily identified at 204.0 m (Fig. 5) and corresponds to a dissolution zone at the base of the Marlboro Clay. This rapid transition is followed by a gradual recovery of carbon isotope values, similar to what is reported from other sections, especially from shelf environments such as Bass River and Wilson Lake (Gibbs et al., 2006a; Sluijs et al., 2007; Sluijs and Brinkhuis, 2009), but dissimilar from the section in Tanzania (Bown and Pearson, 2009), where an abrupt recovery of the $\delta^{13}C$ values suggests the presence of a hiatus. The end of Phase I of the PETM, identified by Rohl et al. (2007) as the onset, peak, and initial recovery of $\delta^{13}C$, is placed at 190.5 m.

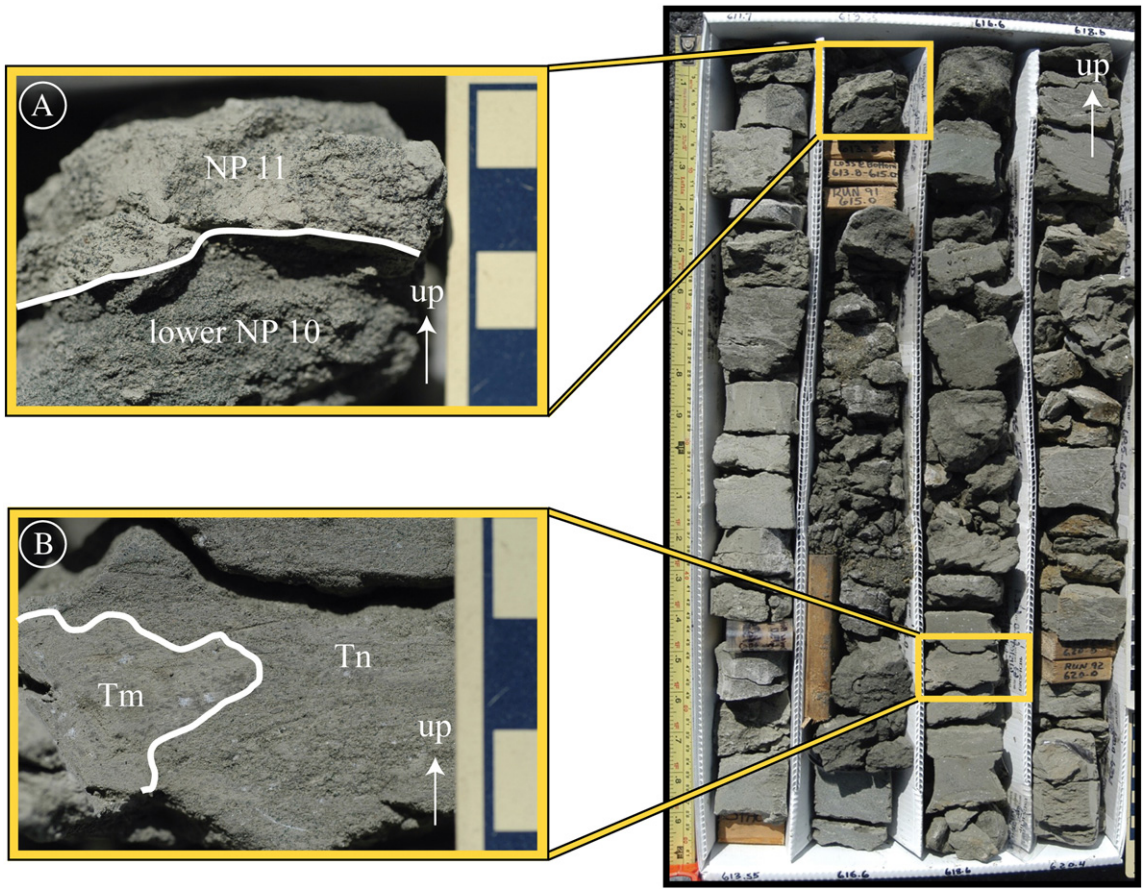

Fig. 4. Photograph of Box 67, from 186.4 m to 189.1 m, containing the Marlboro Clay/Nanjemoy Formation contact in the South Dover Bridge core. A) Contact (white line) between lower Zone NP10 and Zone NP11 at 187.1 m. B) Contact (white line) between the Marlboro Clay (Tm) and the Nanjemoy Formation (Tn) at 188.4 m. Arrows show stratigraphic up.

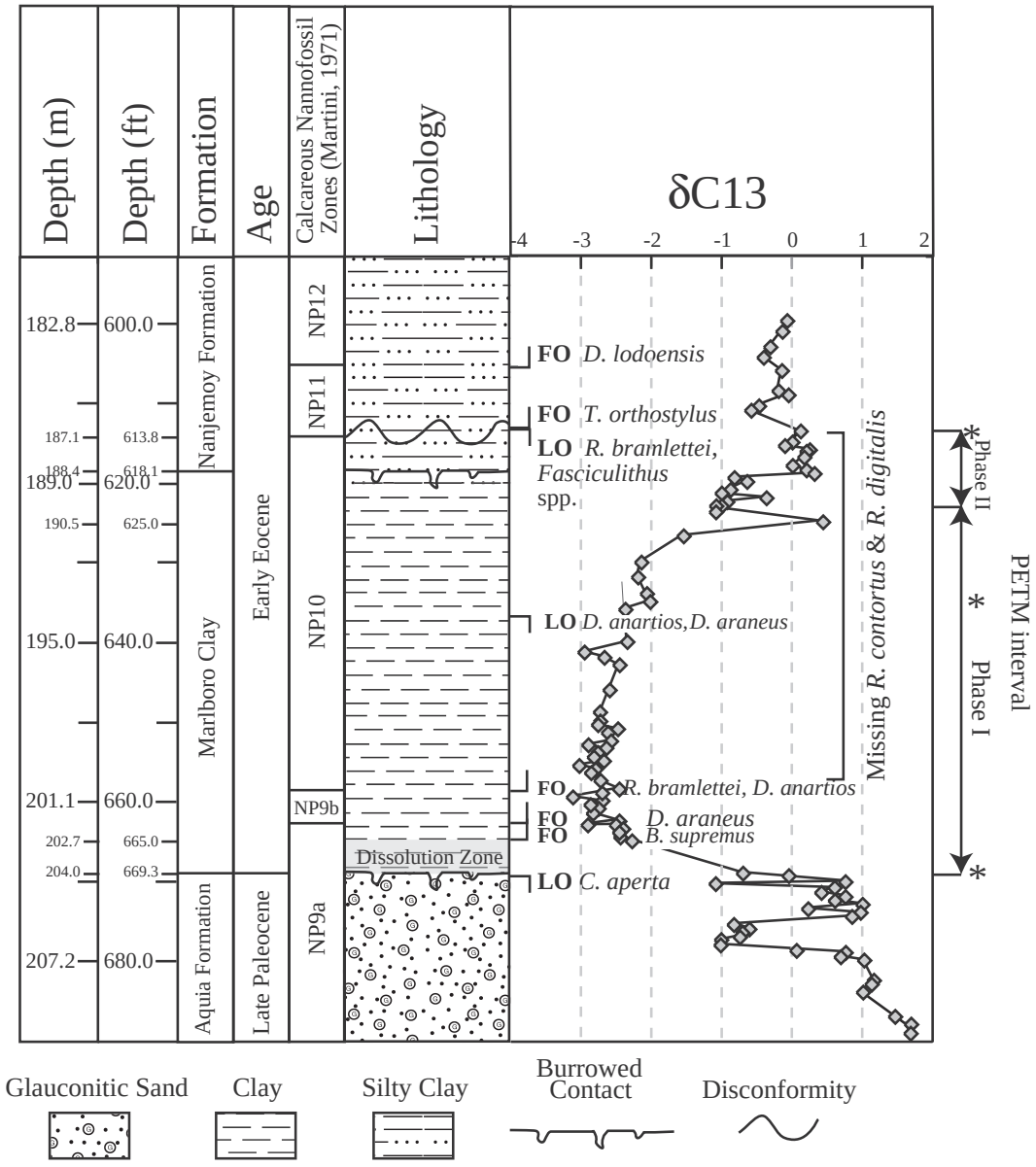

Fig. 5. Stratigraphic column of the Paleocene/Eocene boundary in the South Dover Bridge core, correlated with the carbon isotope excursion graph and first occurrences (FO) and last occurrences (LO) of key taxa. Asterisks (*) denote location of, from bottom to top, the CIE, the beginning of recovery, and the end of the PETM. Calcareous nannofossils zonation is based on the scheme of Martini (1971). Modified from Self-Trail (2011).

The end of Phase II (slow rise in $\delta^{13}C$ and high carbonate) is placed at the unconformable NP10/NP11 boundary at 187.05 m.

4. Material and methods

4.1. Calcareous nannofossils

Fifty-two samples analyzed for calcareous nannofossil content (Table 1; Plates 1 and 2) were taken from the central portion of freshly broken core approximately every 12 cm from 210.0 m (Aquia Formation) into the basal Nanjemoy Formation, which encompasses the entire PETM event. Drilling mud injection, caused by the high pressures needed to cut the dense Marlboro Clay and Nanjemoy Formation, resulted in the formation of thin layers of mixed formation material with drilling fluid; sampling of these intervals for paleontological and/or geochemical analysis was avoided whenever possible.

Slides were prepared from raw material using the double smear slide method of Blair and Watkins (2009) and were examined under cross-polarized and plane light using a Zeiss Axioplan 2 petrographic microscope at 1250× magnification (2000× for details and/or small taxa). An initial semi-quantitative analysis determined biostratigraphy and relative abundance for all species for each slide and allowed for the identification of rare taxa.

For quantitative analysis, each slide was randomly scanned until 400 specimens had been counted and this supplementary data can be accessed online at http://dx.doi.org/10.1016/j.marmicro.2012.05.003. For the PETM interval of the Tethyan Seaway, Kahn and Aubry (2004) identified a short-lived (<170,000 years) excursion assemblage of calcareous nannofossils with anomalous coccolith structure consisting of *Rhomboaster* spp., *Discoaster anartios*, and *D. araneus*, which they called the *Rhomboaster–Discoaster* (RD) assemblage. In the SDB core, the RD assemblage, which is used as a proxy for the PETM event, is present in very minor amounts (<4%). In order to document the relative abundance

Table 1
Depths of samples, in feet and in meters, taken for carbon isotope and calcareous nannofossil assemblage analysis.

Depth (ft)	Depth (m)	dC13	Calcareous nannofossil sample	Depth (ft)	Depth (m)	dC13	Calcareous nannofossil sample	Depth (ft)	Depth (m)	dC13	Calcareous nannofossil sample
600.1	182.9	−0.10		639.0	194.8		X	666.5	203.1		X
601.2	183.2	−0.17		640.1	195.1	−2.37		667.2	203.4		X
603.1	183.8	−0.34		640.8	195.3		X	667.5	203.5		X
604.4	184.2	−0.43	X	641.4	195.5	−2.98		668.0	203.6		X
606.1	184.7	−0.17		642.0	195.7	−2.70	X	668.5	203.8		X
607.0	185.0		X	643.0	196.0	−2.49		669.0	203.9	−0.73	X
608.6	185.5	−0.22		645.0	196.6		X	669.4	204.0	−0.07	
609.1	185.7	−0.08		646.1	196.9	−2.62		669.5	204.1		X
609.8	185.8		X	649.0	197.8	−2.76	X	670.1	204.2	0.73	
610.5	186.1	−0.50	X	650.1	198.2	−2.76	X	670.4	204.3	−1.12	X
611.1	186.3	−0.61		650.5	198.3	−2.79		670.9	204.5	0.57	
613.0	186.8		X	651.0	198.4	−2.53		671.5	204.7	0.39	X
613.7	187.1	0.09	X	651.5	198.6	−2.65		672.0	204.8	0.73	
615.1	187.5	−0.04	X	652.0	198.7		X	672.5	205.0	0.58	
615.5	187.6	−0.13		652.5	198.9	−2.62		673.0	205.1	0.97	
616.0	187.7	0.22		653.0	199.0	−2.93		673.5	205.3	0.20	
616.3	187.8	0.17	X	653.5	199.2	−2.69		674.0	205.4	0.93	
617.0	188.1	0.14		654.0	199.3	−2.80		674.5	205.6	0.83	
618.0	188.4	−0.02		654.5	199.5	−2.85		675.0	205.7		X
618.5	188.5	0.17		655.0	199.6	−2.72		675.5	205.9	−0.86	
619.0	188.7	0.29		655.6	199.8	−3.06	X	676.0	206.0	−0.64	
619.5	188.8	−0.85		656.0	199.9	−2.83		676.5	206.2	−0.74	
619.9	188.9		X	656.5	200.1	−2.89		677.0	206.3	−0.77	
620.0	189.0	−0.67		657.5	200.4	−2.76		677.5	206.5	−1.04	
620.5	189.1		X	658.0	200.5		X	678.0	206.7	−1.04	
621.0	189.3	−0.90		658.5	200.7	−2.50		678.7	206.9	0.03	X
621.5	189.4	−1.02		659.0	200.9	−2.74		679.0	207.0	0.73	
622.0	189.6	−0.40		659.5	201.0	−3.15		679.5	207.1	0.67	
622.5	189.7	−0.96		660.0	201.2	−2.74		680.0	207.3	1.00	
623.0	189.9	−1.09		660.5	201.3	−2.90	X	680.3	207.4		X
623.4	190.0	−1.06	X	661.0	201.5	−2.79		681.0	207.6		X
625.0	190.5	0.41		661.5	201.6	−2.87	X	682.5	208.0	1.14	
626.0	190.8		X	662.0	201.7		X	683.0	208.2	1.11	X
626.8	191.0	−1.58		662.5	201.9	−2.50	X	684.0	208.5	0.98	
630.1	192.1	−2.17	X	663.0	202.1	−2.93	X	686.0	209.1		X
630.8	192.3		X	663.5	202.2	−2.44	X	687.0	209.4	1.44	
632.0	192.6	−2.22		664.0	202.4	−2.50	X	688.0	209.7	1.60	
633.3	193.0		X	664.5	202.5	−2.47	X	689.0	210.0	1.66	X
634.0	193.2	−2.10		665.0	202.7	−2.31	X				
635.0	193.5	−2.05		665.5	202.8		X				
636.0	193.9	−2.40	X	666.0	203.0		X				

changes in species of the RD assemblage, additional counts of all *Rhomboaster* spp., *D. anartios*, and *D. araneus* against 100 *Discoaster* specimens (excluding *D. anartios* and *D. araneus*) were tallied.

4.2. Carbon isotopes

Ninety-four carbonate carbon isotope values were obtained by digestion with 100% phosphoric acid using the method of McCrea (1950) (Table 1). Samples were ground in an agate mortar and pestle until a fine powder was obtained. The carbon isotopes were measured on a Finnigan MAT251. The data are reported in the standard delta notation (δ) in per mil relative to Vienna Peedee Belemnite (VPDB). The 1s standard deviation for the method was determined by repeated analysis of a similar sediment with each batch of samples. For $\delta^{13}C$ $1\sigma = 0.04‰$ n = 13.

5. Results

Calcareous nannofossil taxa before, during, and after the PETM were responding to a suite of ecological variables that were complex and difficult to identify. These variables include but are not necessarily limited to nutrient influx, temperature, salinity, and water clarity at the time of sedimentation. Additionally, post-sedimentation diagenesis can also affect assemblage abundance and variability and create difficulty in identifying primary versus secondary associations between species and/or groups. Thus, in the following sections, assemblages are examined and discussed in stratigraphic order and based on their juxtaposition with the CIE; pre-PETM, syn-PETM, and post-PETM.

5.1. Pre-PETM taxa

In the SDB core, three species (*Toweius eminens*, *T. tovae*, and *Zygodiscus herlyni*) show decreased abundances across the Paleocene/Eocene boundary and one species (*Calciosolenia aperta*) goes extinct (Fig. 6). The relative abundance of *Hornibrookina* spp., a group typically present in trace amounts throughout the Paleocene and Eocene but which occasionally occurs in high abundances, spikes twice in the late Paleocene of SDB: at 210 m (~28%) and at 204.7 m (70%), just below the CIE (Fig. 6). *Chiasmolithus*, a genus long associated with cooler water conditions (Bukry, 1973; Wei and Wise, 1990; Firth and Wise, 1992; Jiang and Wise, 2006), is well-represented by *C. bidens*, which occurs in abundances up to ~17% below the boundary (209.1 m), but then begins a slow decrease in relative abundance until it disappears (204.1 m) during the PETM event. It reoccurs in reduced numbers (<7%) following recovery.

5.2. Syn-PETM taxa

5.2.1. Carbon isotope excursion taxa

The base of the CIE begins at 204.0 m and coincides with the base of a thin dissolution zone that extends to 202.7 m. Excursion taxa, or

those restricted entirely to the PETM interval, first begin to occur in rare abundances at the top of the dissolution zone at 202.7 m (Fig. 7). The first to occur are *Bomolithus supremus*, in abundances no greater than 1.5%, *Coccolithus bownii* (up to 7%), and *Toweius serotinus* (abundance up to 32%). Both *B. supremus* and *C. bownii* decrease in abundance in earliest PETM sediments, but *T. serotinus* increases in relative abundance from less than 1% at the base of the event to 19% at 197.8 m, and reaches its highest abundance at 189.1 m (32%) just below the Marlboro Clay/Nanjemoy contact (Fig. 7). Its last occurrence is recorded at 188.9 m (25%) in the upper Marlboro Clay, just below the contact with the Nanjemoy Formation.

5.2.2. RD assemblage

Kahn and Aubry (2004) identified the *Rhomboaster* spp.–*Discoaster araneus* association (RD assemblage) from sites in the North and South Atlantic Oceans and from the Tethys Seaway and suggested that it is correlative with the earliest CIE. At SDB, taxa of the RD assemblage do not occur simultaneously. Rather, individual species rapidly occur in succession, starting with the first occurrence of *D. araneus*, followed by the co-occurrence of *D. anartios* with *Rhomboaster* spp. (Fig. 8). *Discoaster araneus* has its first occurrence at 201.9 m, and its relative abundance remains low, never getting above 4%. It is very sporadic in occurrence and never becomes a dominant component of the assemblage. In comparison, *D. anartios* is present in every sample after its first occurrence at 200.5 m until its disappearance at 193.9 m. It reaches relative abundance values of 17% at 197.8 m and then begins to decline. By the time that carbon isotope values are beginning to recover at approximately 193.0 m, *D. anartios* is extinct.

Specimens of *Rhomboaster* first occur (<1%) at 200.5 m, coincident with *D. anartios*, and rapidly increase in abundance up section. Two distinctive peaks in relative abundance are identified. The first abundance peak never reaches greater than 15% and represents the rapid onset of warming during the CIE and immediately following the event. The second peak is more pronounced at 26% and coincides with the onset of recovery of the carbon isotopes to more normal

Plate 1. All samples taken in cross-polarized (XPL) light at 2000× magnification. Scale bar = 3 μm.

1. *Bomolithus supremus*, sample N12488, 198.7 m, South Dover Bridge core, MD.
2. *Calciosolenia aperta*, sample N12494, 205.7 m, South Dover Bridge core, MD.
3. *Chiasmolithus bidens*, sample N12493, 204.7 m, South Dover Bridge core, MD.
4, 5. *Coccolithus bownii*, sample N12488, 198.7 m, South Dover Bridge core, MD.
6. *Coronocyclus bramlettei*, sample N12476, 186.8 m, South Dover Bridge core, MD.
7. *Discoaster anartios*, sample N12488, 198.7 m, South Dover Bridge core, MD.
8. *Discoaster multiradiatus*, sample N12493, 204.7 m, South Dover Bridge core, MD.
9. *Ellipsolithus distichus*, sample N12493, 204.7 m, South Dover Bridge core, MD.
10, 15. *Fasciculithus involutus*, sample N12496, 207.6 m, South Dover Bridge core, MD.
11. *Hornibrookina arca*, sample N12493, 204.7 m, South Dover Bridge core, MD.
12. *Neochiastozygus junctus*, sample N12422, 201.3 m, South Dover Bridge core, MD.
13, 14. *Rhomboaster* spp., sample N12482, 193.0 m, South Dover Bridge core, MD.
16. *Prinsius bisulcus*, sample N12495, 206.9 m, South Dover Bridge core, MD.
17, 18. *Semihololithus biscayae*, sample N12495, 206.9 m, South Dover Bridge core, MD.
19. *Toweius callosus*, sample N12415, 178.3 m, South Dover Bridge core, MD.
20. *Toweius callosus*, sample N12476, 186.8 m, South Dover Bridge core, MD.
21. *Toweius eminens*, sample N12493, 204.7 m, South Dover Bridge core, MD.
22. *Toweius occultatus*, sample N12415, 178.3 m, South Dover Bridge core, MD.
23. *Toweius pertusus*, sample N12494, 205.7 m, South Dover Bridge core, MD.
24. *Toweius serotinus*, sample N12488, 198.7 m, South Dover Bridge core, MD.
25. *Toweius tovae*, sample N12493, 204.7 m, South Dover Bridge core, MD.
26, 27. *Zygodiscus herlyni*, sample N12493, 204.7 m, South Dover Bridge core, MD.
28, 29. *Zygodiscus sheldoniae*, sample N12493, 207.7 m, South Dover Bridge core, MD.
30. *Zygrhablithus bijugatus*, sample N12476, 186.8 m, South Dover Bridge core, MD.

Plate 2. All samples taken in cross-polarized (XPL) light at 2000× magnification. Scale bar = 3 μm. (see on page 10)

1. *Calcidiscus? parvicrucis*, sample N12416, 181.6 m, South Dover Bridge core, MD.
2. *Calcidiscus? parvicrucis*, sample N12473, 184.2 m, South Dover Bridge core, MD.
3, 4. *Discoaster araneus*, sample N12422, 201.3 m, South Dover Bridge core, MD.
5. *Discoaster araneus*, sample N12422, 201.3 m, South Dover Bridge core, MD.
6. *Cycligelosphaera reinhardtii*, sample 12499, 210.0 m, South Dover Bridge core, MD.
7. *Cycligelosphaera reinhardtii*, sample 12499, 210.0 m, South Dover Bridge core, MD.
8. *Discoaster kuepperi*, sample 12416, 181.6 m, South Dover Bridge core, MD.
9. *Discoaster kuepperi*, side view, sample 12416, 181.6 South Dover Bridge core, MD.
10. *Discoaster lodoensis*, sample 12416, 181.6 m, South Dover Bridge core, MD.
11, 12. *Discoaster falcatus*, sample N12495, 206.9 m, South Dover Bridge core, MD.
13, 14. *Discoaster falcatus*, sample N12495, 206.9 m, South Dover Bridge core, MD.
15. *Fasciculithus mitreus*, sample N12495, 206.9 m, South Dover Bridge core, MD.
16. *Fasciculithus involutus*, sample N12495, 206.9 m, South Dover Bridge core, MD.
17. *Fasciculithus involutus*, sample N12495, 206.9 m, South Dover Bridge core, MD.
18. *Fasciculithus richardii*, sample N12495, 206.9 m, South Dover Bridge core, MD.
19. *Fasciculithus richardii*, sample N12495, 206.9 m, South Dover Bridge core, MD.
20. *Fasciculithus thomasii*, sample N12495, 206.9 m, South Dover Bridge core, MD.
21. *Fasciculithus tympaniformis*, sample N12499, 210.0 m, South Dover Bridge core, MD.
22. *Markalius apertus*, sample N12473, 184.2 m, South Dover Bridge core, MD.
23. *Markalius apertus*, sample N12473, 184.2 m, South Dover Bridge core, MD.
24. *Markalius inversus*, sample N12416, 181.6 m, South Dover Bridge core, MD.
25. *Markalius inversus*, sample N12416, 181.6 m, South Dover Bridge core, MD.
26. *Toweius? magnicrassus*, sample N12473, 184.2 m, South Dover Bridge core, MD.
27. *Toweius? magnicrassus*, sample N12473, 184.2 m, South Dover Bridge core, MD.
28. *Tribrachiatus orthostylus*, sample N12416, 181.6 m, South Dover Bridge core, MD.
29. *Tribrachiatus orthostylus*, sample N12416, 181.6 m, South Dover Bridge core, MD.
30. *Markalius inversus*, sample N12416, 181.6 m, South Dover Bridge core, MD.

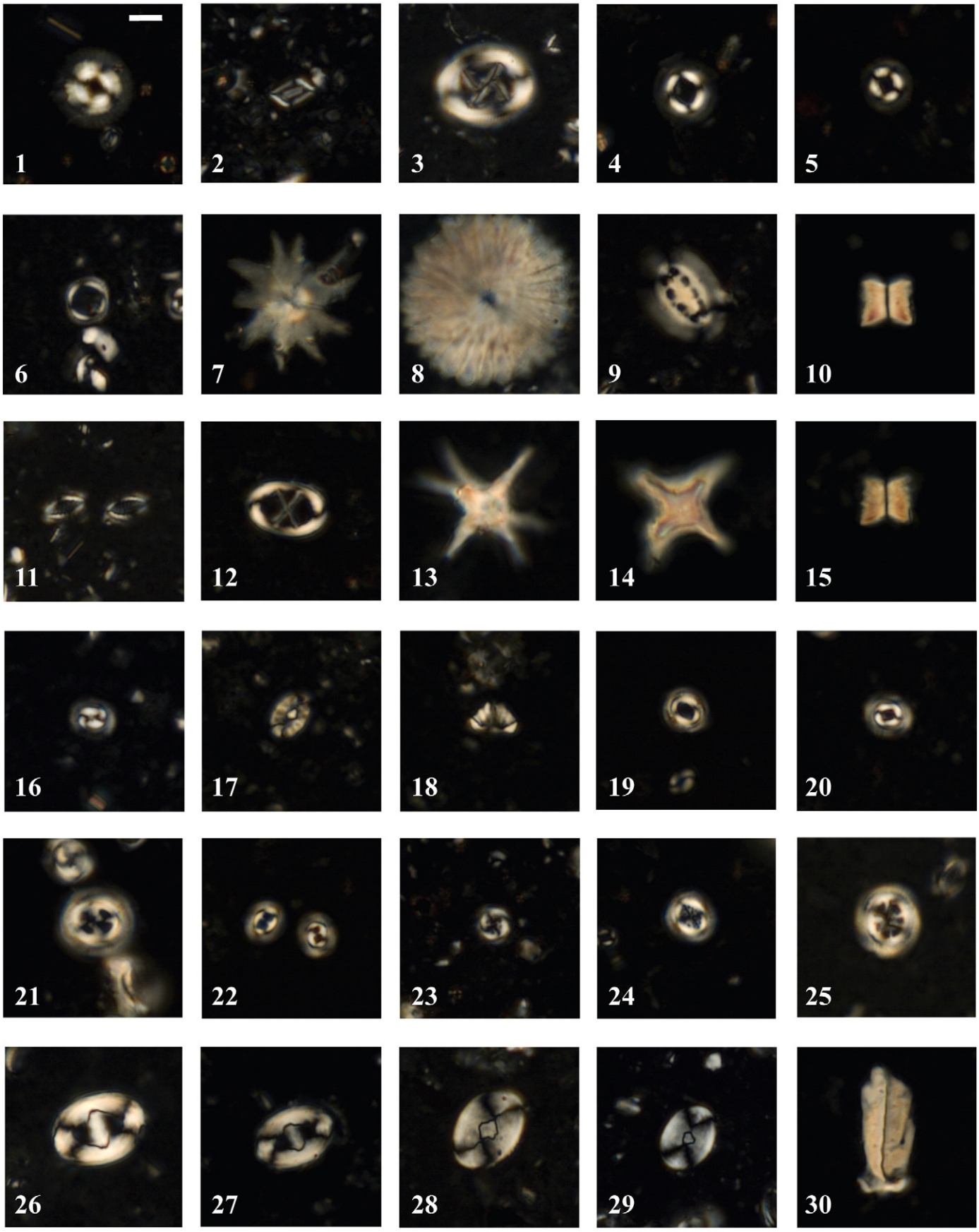
1
2
3
4
5
6
7
8
9
10
11
12
13
14
15
16
17
18
19
20
21
22
23
24
25
26
27
28
29
30

Plate 1.

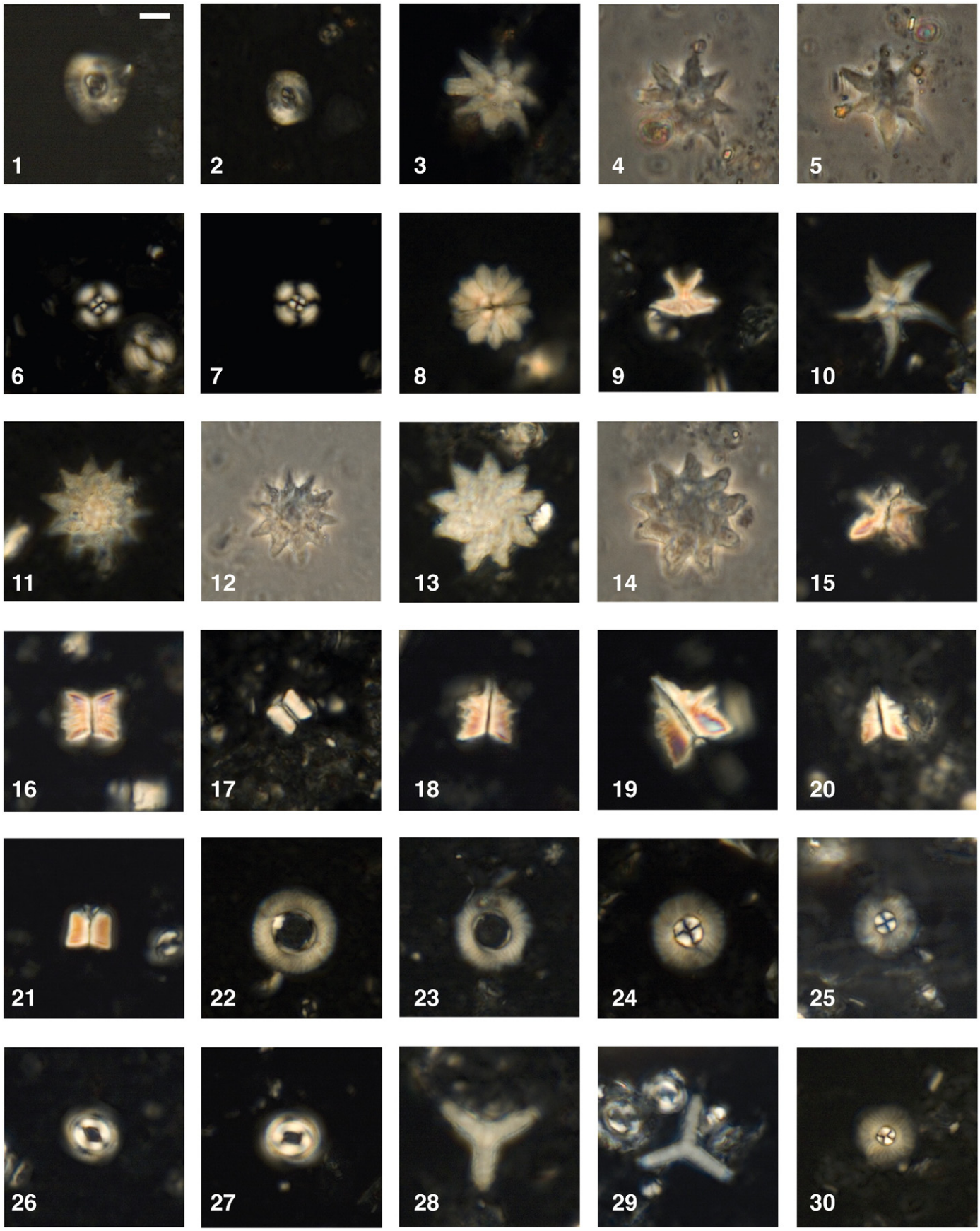

Plate 2 (*caption on page 8*).

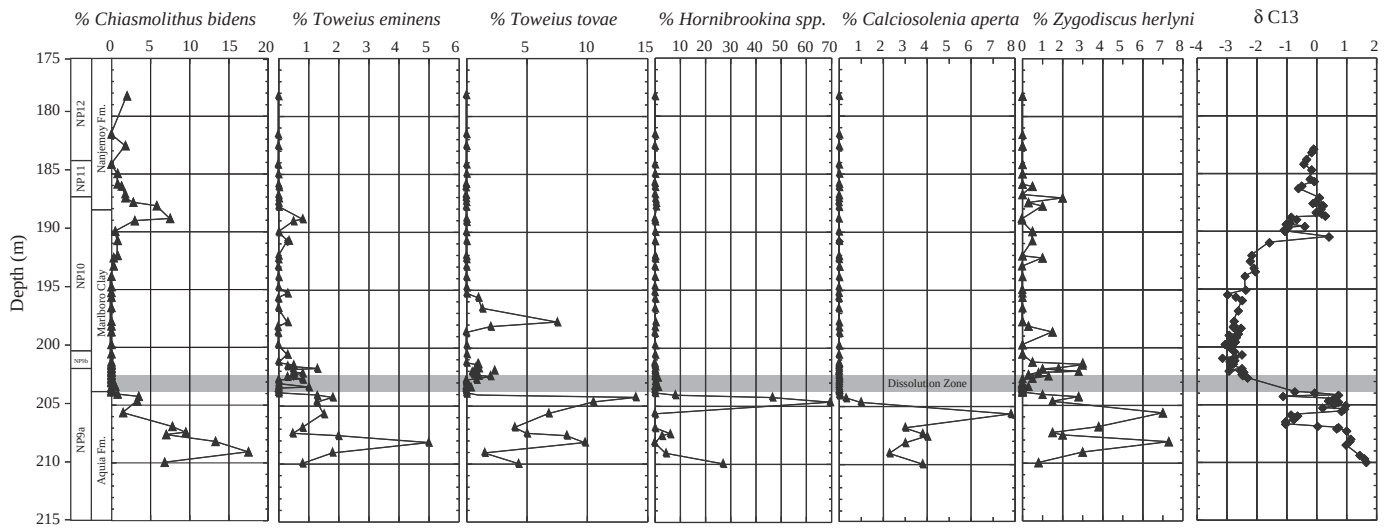

Fig. 6. Relative abundance graphs of pre-PETM taxa that show a decrease in abundance during the PETM. This is followed by a concomitant increase in the abundance of some taxa following the event (*C. bidens, Z. bijugatus, C. parvicrucis*) or a spike in abundance prior to the event (*Hornibrookina* spp.). Shadowed interval indicates a zone of dissolution.

conditions (Fig. 8). Specimens of *Rhomboaster* are present in the assemblage up to 187.5 m, where a disconformable contact between Zones NP10 and NP11 truncate the PETM event.

The RD assemblage is never very abundant in the overall calcareous nannofossil population. Relative abundance of the group when compared to the total assemblage never reaches greater than 4%. Individually, *D. anartios* never reaches abundances greater than 1.5%, *Rhomboaster* spp. never get above 2.5%, and *D. araneus* is always less than 1% of the total calcareous nannofossil assemblage.

5.3. Dissolution resistant and opportunist taxa

In the SDB core, *Discoaster multiradiatus*, *Ellipsolithus distichus*, and *Fasciculithus* spp. are present in abundances less than 5% below the Paleocene/Eocene boundary (Fig. 9), but peak to 21%, 5%, and 14%, respectively, in the dissolution zone near the base of the PETM (samples at 203.9 m and 203.4 m), reflecting the fact that these species are dissolution resistant. The abundances of these taxa fluctuate between 0 and 7% throughout the PETM and abruptly decrease to <1% at the Marlboro

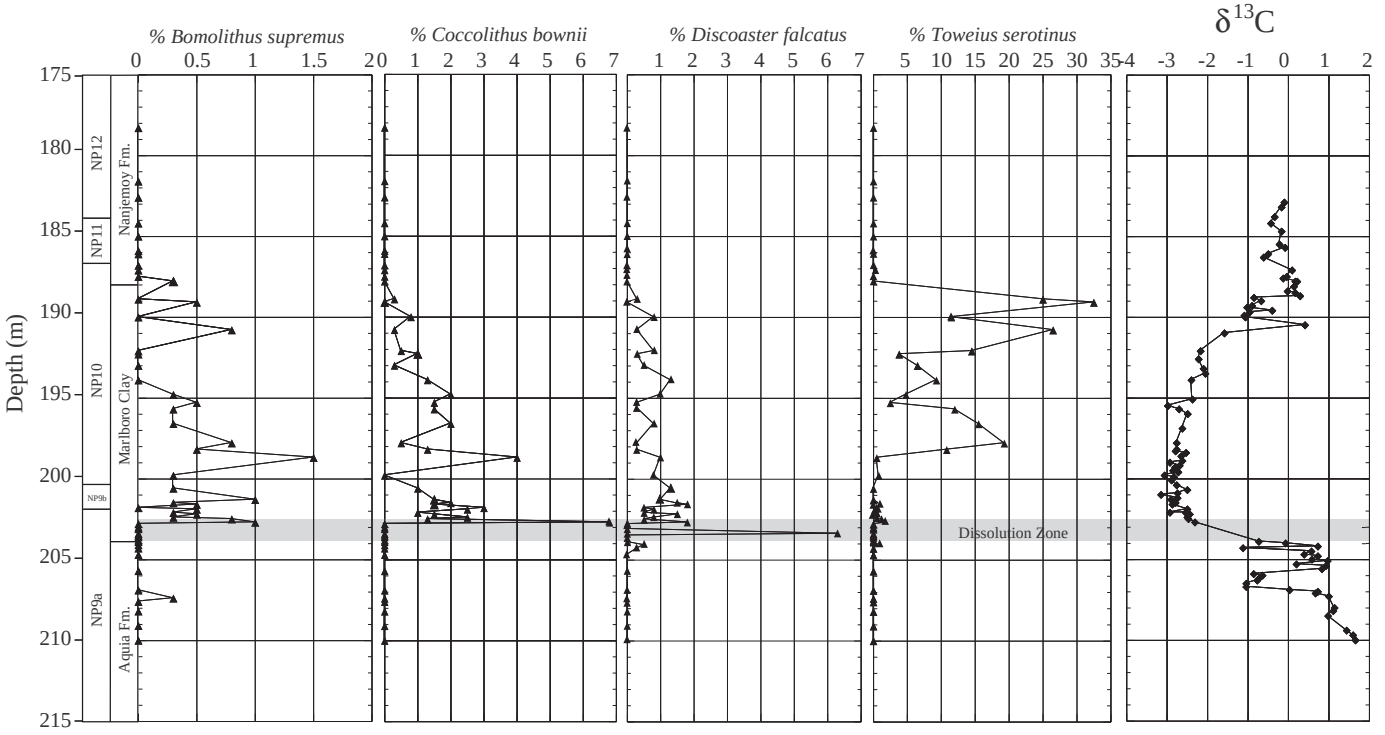

Fig. 7. Relative abundance graphs of excursion taxa, or those species that appear to be restricted to the PETM interval, compared against the $\delta^{13}C$ curve. *Bomolithus supremus, D. falcatus*, and *T. serotinus* are present in abundances <1% just prior to the event, but this may represent minor bioturbation across the boundary. The spike in percent abundance of *D. falcatus* to ~6% in the dissolution interval suggests that *D. falcatus* is a dissolution-resistant species. Shadowed interval indicates a zone of dissolution.

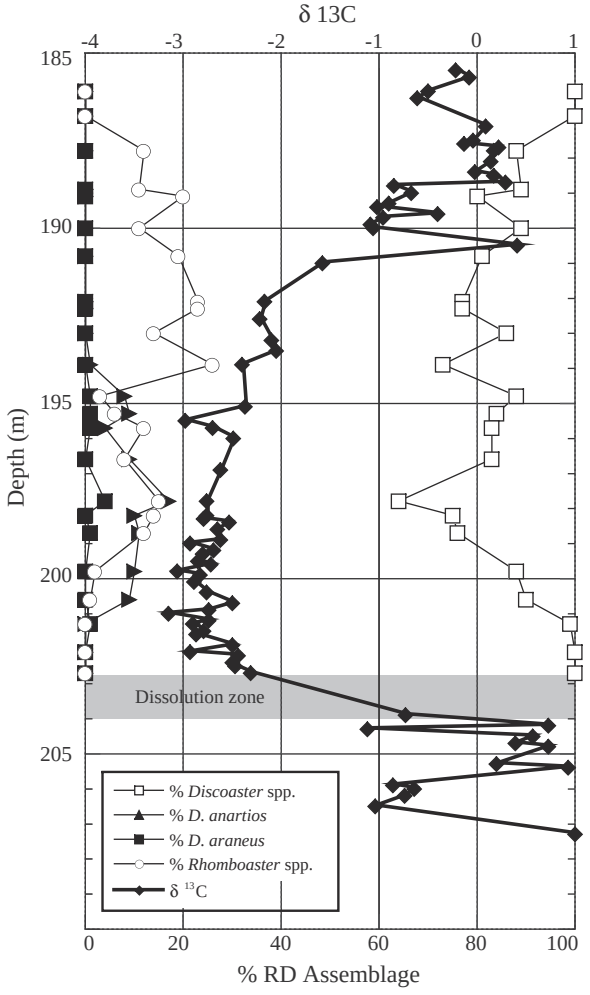

Fig. 8. Graph showing the relative abundance of the RD assemblage (*D. araneus*, *D. anartios*, *Rhomboaster* spp.) plotted against percent abundance of 100 *Discoaster* spp. (minus *D. araneus* and *D. anartios*) and the $\delta^{13}C$ curve. Note that ecophenotypic species such as *D. araneus* and *D. anartios* disappear at the point the $\delta^{13}C$ curve begins to show recovery.

Clay/Nanjemoy Formation boundary (Fig. 9). *Coronocyclus bramlettei* and *Neochiastozygus junctus* are present in trace amounts below and above the PETM interval but increase to 6% and 12%, respectively, during the PETM interval. These two species are not present in the two samples from the dissolution zone (203.9 m and 203.4 m).

5.4. Toweius/Coccolithus association

Species of the genus *Toweius* dominate the calcareous nannofossil assemblage before, during and after the PETM event, showing decreased abundances only just before the event (Fig. 10). Abundances range between 40 and 60% below 192 m and increase to between 60 and 80% above this horizon, not quite coinciding with the Marlboro Clay/Nanjemoy Formation contact. In contrast, percent abundance of *Coccolithus* is less than 20% in upper Paleocene sediments and increases to between 20 and 40% during the PETM, gradually declining to pre-PETM levels.

5.5. Syn- and post-PETM taxa

5.5.1. Genus Toweius

Examination of individual species of *Toweius* shows changing dominance patterns throughout the late Paleocene and early Eocene. *Toweius pertusus*, which most likely includes the species *T. rotundus* as used by Bown and Pearson (2009), is the dominant species and ranges between 30 and 50% throughout the PETM interval (Fig. 11). It decreases sharply in abundance at the Marlboro Clay/Nanjemoy Formation contact.

Toweius eminens and *T. tovae* have pre-PETM abundances up to 5% and 14%, respectively, but decrease in abundance dramatically across the P/E boundary (Fig. 11). Once past the PETM, *T. eminens* is present up to the Marlboro Clay/Nanjemoy contact only in rare amounts (<1%), where it goes extinct, and *Toweius tovae* is sporadically present to the NP9/10 boundary, occasionally reaching abundances of up to ~7% of the assemblage.

Toweius serotinus is the only species in this genus that is restricted to the PETM interval and most likely is an excursion taxa. It is present in only trace amounts during the basal PETM, but rapidly increases to over 30% relative abundance of the assemblage near the top of the

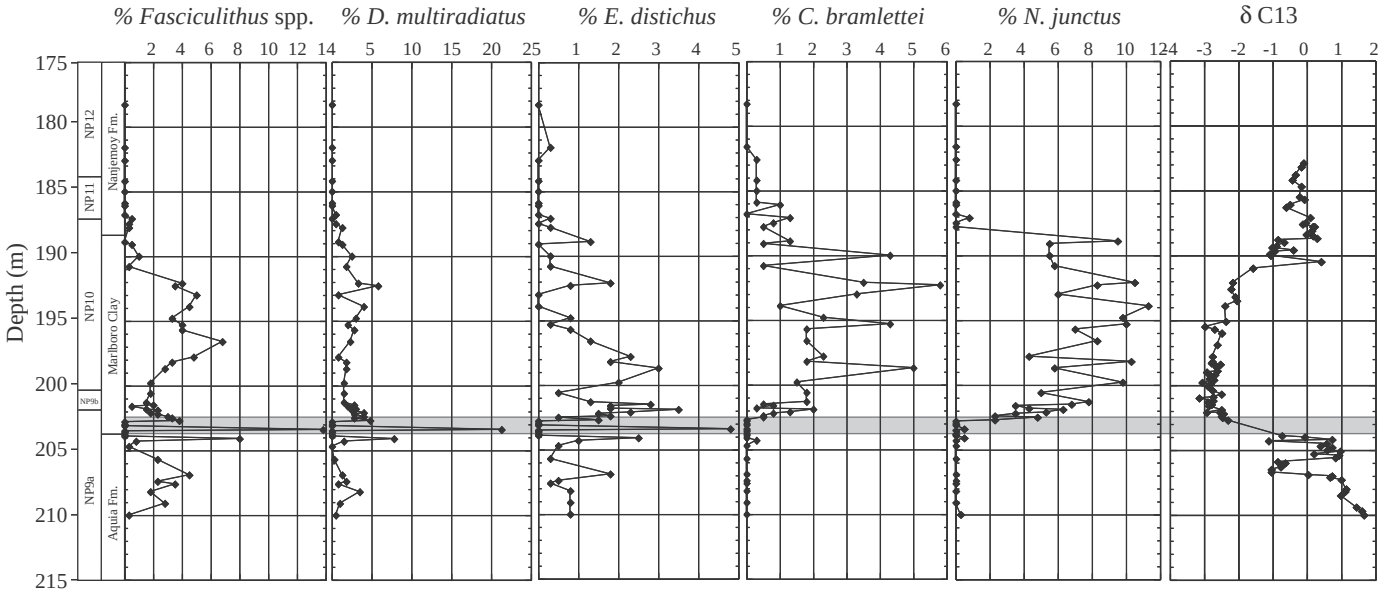

Fig. 9. Relative abundance graphs of PETM taxa; those species that show an increase in abundance during the event, but are not restricted to the duration of the event. Strong peaks in percent abundance of *Fasciculithus* spp., *D. multiradiatus*, and *E. distichus* in the dissolution interval suggest these species are dissolution resistant and that their signal may, in part, represent preservation. Shadowed interval indicates a zone of dissolution.

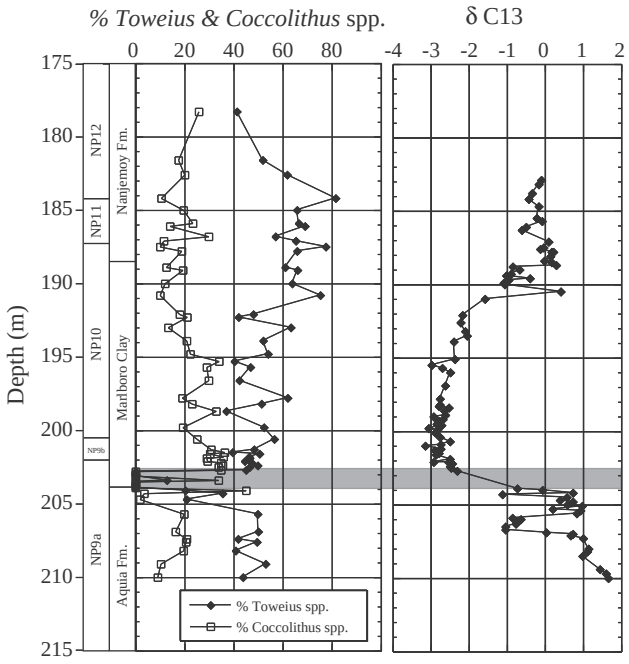

Fig. 10. Relative abundance graphs of *Toweius* spp. and *Coccolithus* spp. plotted against the $\delta^{13}C$ curve. *Toweius* spp. dominated throughout the Paleocene and Eocene at this site. Shadowed interval indicates a zone of dissolution.

PETM interval (Fig. 11). Its abundance is highest during the recovery phase, and its last occurrence is at the Marlboro Clay/Nanjemoy contact.

Both *Toweius callosus* and *T. occultatus* are present in minor amounts in sediments of latest Paleocene and earliest Eocene age, before increasing in abundance. *Toweius callosus* increases rapidly in relative abundance (60%) to dominate the assemblage at the same time that *T. serotinus* disappears, although the exact nature of their relative dominance and decline is unknown due to the presence of a disconformity. Abundances of *T. occultatus* reach up to 5% throughout the PETM interval and increase to approximately 40% in the Nanjemoy Formation with the concomitant decline in *T. callosus* (Fig. 11).

6. Discussion

One of the key problems in interpretation of PETM nannoplankton assemblages is that paleoenvironmental conditions and variables were rapidly changing at the same time, and separating the impact that each of these variables had on the assemblage is difficult. Typically, the ecology of calcareous nannoplankton is inferred from their paleogeographic distributions; tropical species are thought to be adapted to warm-water and high-latitude species to cold water, coastal species are adapted to eutrophic conditions and open-ocean species to oligotrophic conditions. However, the location of the SDB core on the continental shelf meant that this site was characterized by rapid changes in nutrient and freshwater influx, temperature, salinity, sediment influx, and pH levels during the PETM. Thus, separating the effects on a fossil assemblage of changing temperature from increasing salinity, for example, is particularly challenging.

Gibbs et al. (2006b), their Table S4) and Bown and Pearson (2009, their Table 2) summarize the inferred ecologic niche of key calcareous nannofossil species or groups based on the work of multiple authors, noting that in many cases the preferences of taxa are not well understood. In this paper, we use these inferred niches as a starting point to assess the response of the calcareous nannofossil assemblage at SDB to changing environmental conditions during the PETM. However, it is clear that in some cases, the ecologic assignment previously given does not work, often because niche assignment was given to an entire genus (e.g. *Toweius*) rather than to individual species within a genus (see discussion below). The placement of the SDB core, only approximately 65 miles from the paleoshoreline, provides an opportunity to assess the response of calcareous nannoplankton at the species level to rapidly changing paleoceanographic conditions during the PETM. Where a previous ecologic assessment clearly does not work on assemblages in SDB, we use other sedimentologic or environmental parameters as a means to try to understand species response to changing conditions.

6.1. Sedimentation in the Salisbury Basin

Historically, the depositional history of the Marlboro Clay has been difficult to determine. The rapid changeover from the clearly marine glauconite-rich, illite–smectite dominated muddy sands of the Paleocene Aquia Formation below to the kaolinite-rich silty clay of the

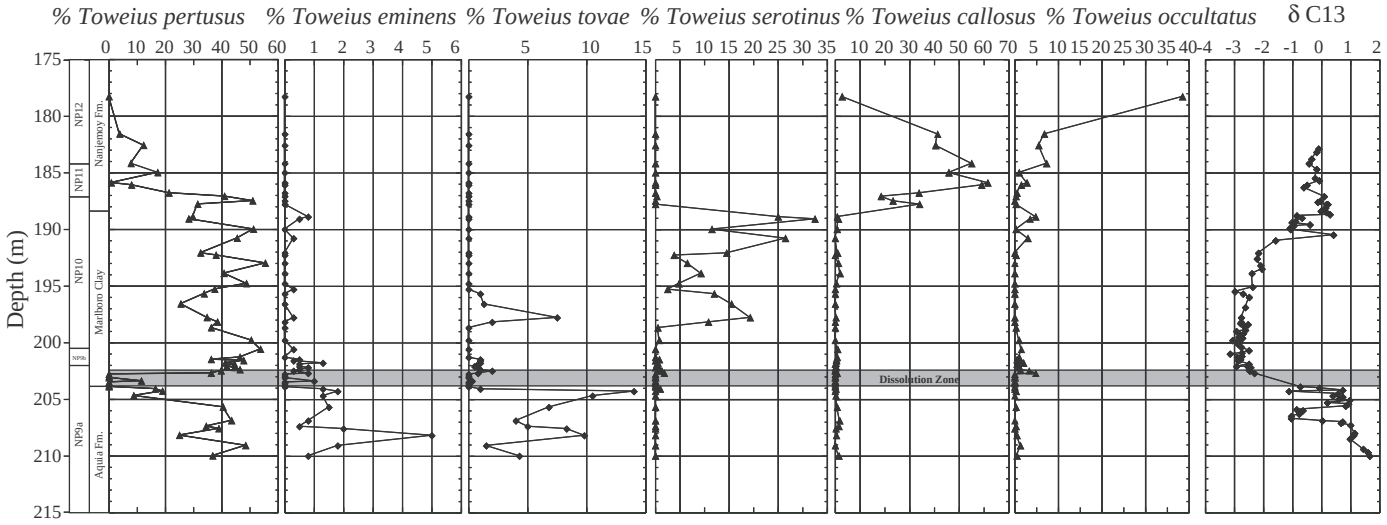

Fig. 11. Relative abundance graphs of the *Toweius* genus. While *T. pertusus* appears to be a generalist, *T. eminens* and *T. tovae* clearly show a stronger affinity for cooler water, mesotrophic conditions, and *T. serotinus* clearly shows a strong preference for warm-water, eutrophic conditions. The increased abundance of *T. callosus* and *T. occultatus* during a period of extreme warmth but decreased continental runoff suggests these species preferred warm-water mesotrophic conditions. Shadowed interval indicates a zone of dissolution.

early Eocene Marlboro Clay makes it difficult to determine the exact environment of deposition. The presence of marine benthic and planktonic foraminifera (Gibson et al., 1980), calcareous nannofossils (Gibson and Bybell, 1994a; Self-Trail, 2011), and dinocysts (Sluijs and Brinkhuis, 2009) in all three formations clearly indicates deposition in a marine setting, and a middle to outer neritic depositional environment is inferred based on microfossil assemblages. High terrestrial runoff into the Salisbury Embayment, as evidenced by the increase in fern spores and terrestrial opaques, the increased kaolinite content, and magnetofossil-to-detrital ratios, (Frederiksen, 1979; Gibson et al., 2000; Kopp et al., 2009; Willard et al., 2009) was most likely induced by a humid warm climate, and suggests that a significant volume of freshwater was introduced into the Salisbury Basin at the Paleocene/Eocene boundary during the carbon isotope excursion. This probably resulted in an initial increase in the nutrient availability to the site, thus increasing fertility. Therefore, it is reasonable to assume that conditions in the Salisbury Embayment were mesotrophic to eutrophic during the initial phase of the hyperthermal event, and that the dramatic increase in abundance of species with uncertain trophic preferences (*Coronocyclus bramlettei, Neochiastozygus junctus, Bomolithus supremus, Toweius serotinus*) is related to nutrient influx and/or changing temperature.

The isopach map of the Marlboro Clay suggests that deposition of sediments in the Salisbury Basin was greatest in the region of the SDB core (Fig. 2). The source of silt and clay to the region during the Paleogene is thought to be paleo-river systems that dominated the region, and were situated near the present Potomac and Susquehanna Rivers (Kopp et al., 2009) or the more northerly Delaware River. Thickness of the Marlboro Clay suggests that the northernmost paleo-river systems were the dominating depositional force during the Paleogene, as evidenced by the presence of the 10 m isopach near the western edge of the formation (Fig. 2). The southernmost paleo-river system contributed less to the system, as evidenced by the thinner isopach lines near the Fall Line. Truncation or thinning of the Marlboro Clay occurred either on the uplifted sides of faults (Mixon and Powars, 1984; Kopp et al., 2009) or occurred due to stripping of sediment during sea level regression following the Eocene hyperthermal events.

Using the astronomically-calibrated age models of Rohl et al. (2007), and based on a thickness of the PETM section of 16.9 m at the SDB site, the estimated sedimentation rate for the PETM at the SDB site is 99.4 m/My (9.9 cm/ky), over double the 40 m/My sedimentation rates recorded by Bown and Pearson (2009) for TDP Site 14 in Tanzania, but similar to estimates from the Bass River and

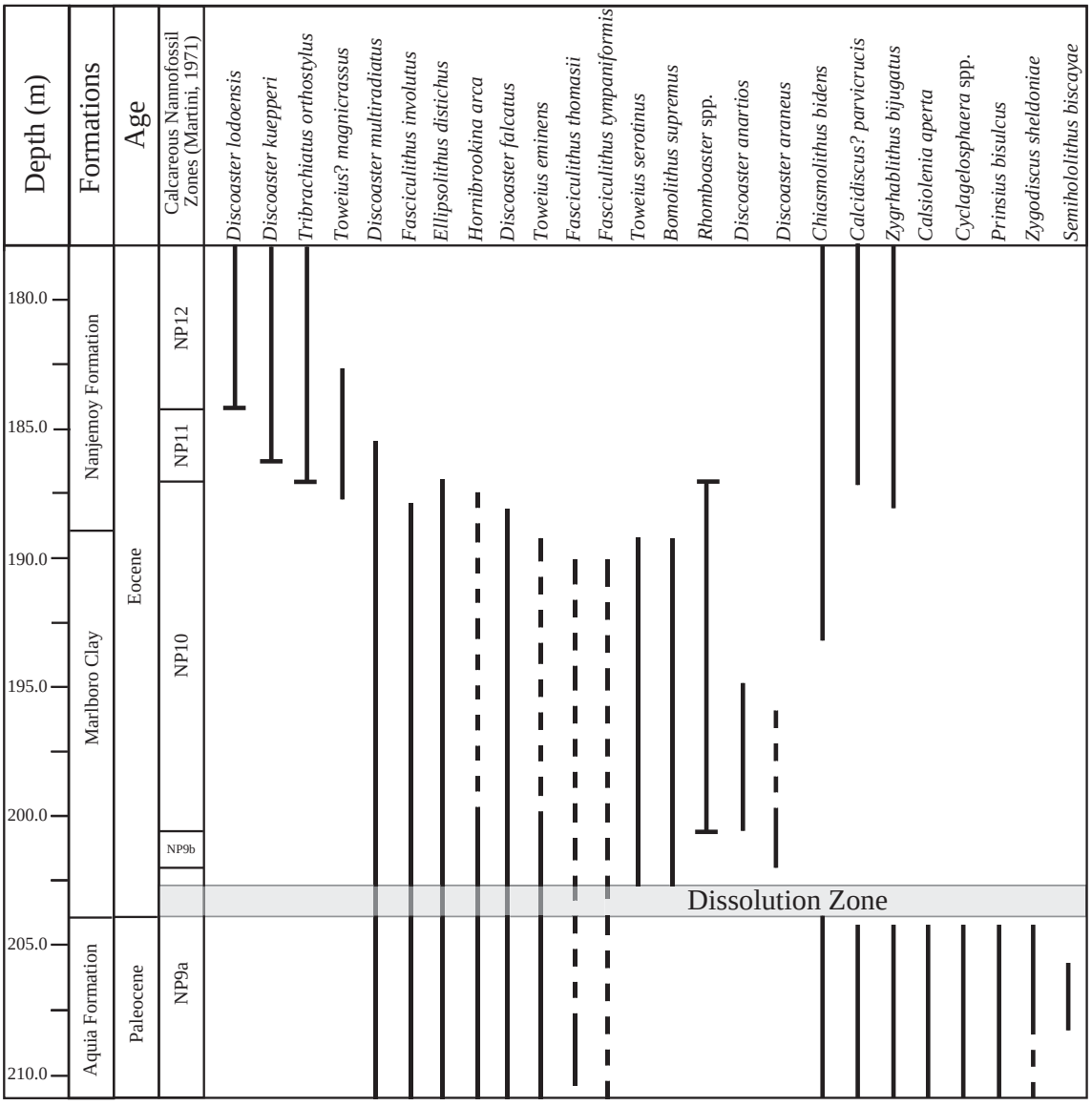

Fig. 12. Partial range chart showing the relative first and last occurrences of important taxa discussed in this paper.

Wilson Lake cores from the New Jersey shelf (Sluijs and Brinkhuis, 2009). These rates, based on the estimated duration of the hyperthermal coupled with biostratigraphic age control, are greater than the "low sedimentary rates" proposed by Gibson and Bybell (1994a) for the regional extent of the Marlboro Clay, but less than the 25.6–29.6 cm/ky (256–296 m/My) proposed by Kopp et al. (2009) for SDB, who used the porosity vs. depth curves of Van Sickle et al. (2004) for the decompaction of sediments to estimate sedimentation rates. Such high sedimentation rates, coupled with evidence of freshwater influx in the form of fern spores and terrestrial opaques (Willard et al., 2009), support the theory that the Marlboro Clay represents the distal end of a tropical river-dominated shelf setting.

6.2. Biostratigraphy

Transition from the Paleocene into the Eocene is characterized in the calcareous nannofossil assemblage by the last occurrences of *C. aperta*, *Prinsius bisulcus*, *Cyclagelosphaera* spp., and *Semihololithus biscayae*, a floral turnover that has been documented at other PETM sites (Bybell and Self-Trail, 1995; Angori and Monechi, 1996; Schmitz et al., 1997; Monechi et al., 2000; Tremolada and Bralower, 2004; Gibbs et al., 2006a; Bown and Pearson, 2009) (Fig. 12). In the SDB core, there is a minor floral turnover at the disconformable Aquia/Marlboro contact, suggesting a very short hiatus. A hiatus is also present in the lower Eocene sediments of the SDB core as evidenced by the absence of the calcareous nannofossil species *Rhomboaster digitalis* and *R. contortus* and by the absence of key dinoflagellate species (Edwards, pers. comm. 2011). The end of the PETM (~55.33 Ma), which lasted approximately 170 kyrs (Rohl et al., 2007), is at 187.05 m and corresponds to the first occurrence of *Tribrachiatus orthostylus* (~53.4 Ma; Raffi et al., 2005) which marks the base of Zone NP11; thus, a hiatus of <1.0 My is recorded in the SDB core, and the top of Phase II (recovery) is most likely truncated.

Bown and Pearson (2009) identified 12 species that have their last occurrences at or near the PETM onset from Tanzania and around the world. In the SDB core, we identify eight species that have either permanent or temporary last occurrences associated with the PETM (Fig. 12). *Calciosolenia aperta, P. bisulcus,* and *Zygodiscus sheldoniae* last occur at 204.3 m, just below the onset of the CIE, and most likely represent a true extinction event. The last occurrence (LO) of *C. aperta* has been recorded from various sections (Bybell and Self-Trail, 1995; Angori and Monechi, 1996; Monechi et al., 2000; Gibbs et al., 2006a; Bown and Pearson, 2009), as has *P. bisulcus* (Tremolada and Bralower, 2004; Gibbs et al., 2006a; Bown and Pearson, 2009). However, *Z. sheldoniae*, a fairly recently described species, has only been identified from Tanzania (Bown, 2005), New Jersey (Gibbs et al., 2006b) and Maryland (Self-Trail, 2011), so its range is still uncertain. The preservation potential of these species is moderate, even for *C. aperta*, whose outer rim typically survives dissolution even if the interior laths are gone. This suggests that their disappearance at the P/E boundary is real and not an artifact related to dissolution. The LO of *S. biscayae* occurs at 205.7 m in the SDB core, just below the LO's of the other species. This LO has also been documented by Bown and Pearson (2009) and Schmitz et al. (1997). The low preservation potential of the holococcoliths probably makes this species unreliable as a marker species, but its presence clearly indicates a Paleocene age. The lowest common occurrence (LCO) of *Markalius apertus* may also prove to be a useful marker event. This species occurs with frequent abundance up until the CIE, where its occurrence becomes sporadic throughout the PETM interval.

The 1.35 m interval from the Marlboro Clay/Nanjemoy contact (188.4 m) to the NP10/NP11 contact (187.05 m; Fig. 4) represents a return to "near normal" sedimentation and environmental conditions at the end of the PETM (recovery Phase II). Increased abundance of burrows, increased glauconite production, and shell fragments all suggest that bottom waters were increasing in oxygen content and that a variety of life forms was able to survive in this region. Abundances of *Rhomboaster* spp. continued to decrease from their peak in the upper 6 m of the Marlboro Clay, dropping to 0% at the base of Zone NP11. These assemblage and lithologic changes coincide with an increase in carbon isotope values (averaging +0.08‰) during this interval, values only slightly lower than those obtained from the Aquia Formation prior to the CIE. This trend toward more positive values characterizes paleoceanographic recovery of the region following the hyperthermal event (Fig. 5).

6.3. Salinity

A consistently high Shannon diversity index and species richness (Fig. 13) at SDB suggests that increased productivity, rather than

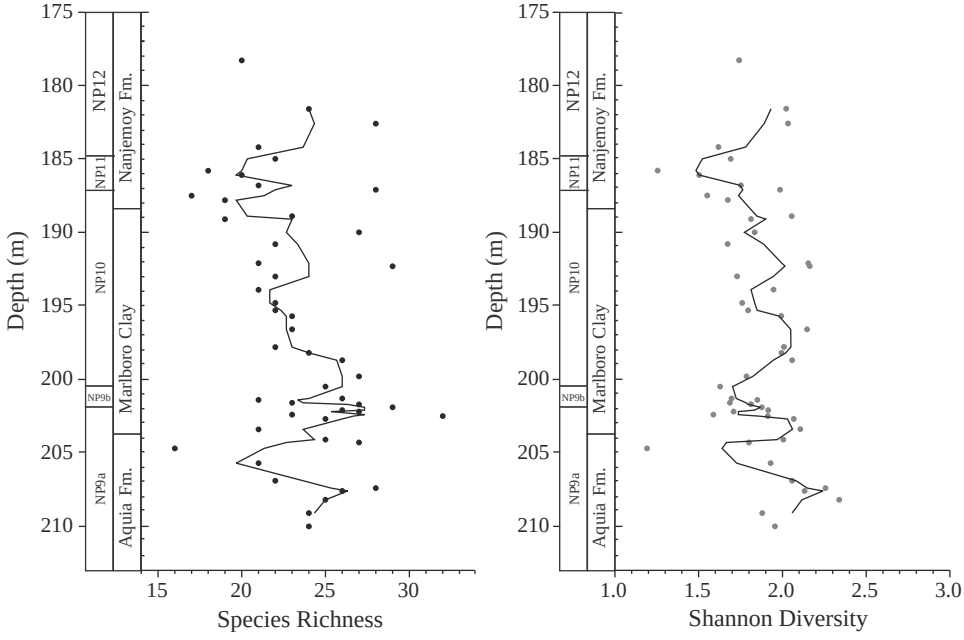

Fig. 13. Calcareous nannofossil species richness and Shannon diversity for the South Dover Bridge core. Solid line indicates a 3 point running average of the dataset.

variation in salinity, played a more dominant role in controlling the assemblage at this site. Increased precipitation rates, as evidenced by the high sedimentation rates of the Marlboro Clay, high percentage of kaolinite, and influx of fern spores at the base of the CIE, undoubtedly brought increased nutrients and fresh water into the Salisbury Basin from the nearby continent. However, Shannon diversity remains relatively constant throughout the PETM, excepting in the dissolution zone at the base of the CIE, suggesting that this site did not experience a dramatic decrease in salinity associated with freshwater influx. Rather, the high biological productivity and accumulation rates associated with SDB suggest that the nannofossil assemblages had access to fully marine conditions, with terrestrially sourced nutrient availability. Gibbs et al. (2006a) report similar results from the nearby Wilson Lake core of New Jersey, where they record an overall increase in productivity during the onset and peak of the PETM. Wilson Lake, however, records a sustained, if minor, decrease in the Shannon diversity across the CIE, suggesting that its slightly closer proximity to the paleoshoreline (35 miles as opposed to 65 miles) and its closer proximity to the sediment source(s) (ancestral Delaware and/or Susquehanna Rivers) may have resulted in a greater impact to the phytoplankton community with regards to salinity variations. In contrast, the greater distance of the SDB core from the sediment source, and thus from the major source of freshwater influx, shielded the site from significant variations in salinity.

6.4. Paleoecology

A mini-excursion of the carbon isotope signal at 206.7–205.9 m, is interpreted as a possible precursor to the main hyperthermal event, and is representative of destabilization of the atmospheric/oceanographic system just prior to the CIE. This brief warming episode may have resulted in a temporary increase in precipitation, which would have increased continental runoff, and hence surface water fertility and productivity just prior to the CIE. The dramatic increase in the abundance of *Hornibrookina arca* (70% at 204.7 m) immediately following this mini-excursion, a species belonging to a genus long thought to have cooler water affinities, supports the interpretation of a return to cooler water conditions following the mini-excursion. However, although species of *Hornibrookina* have previously been used to document cool-water mass boundaries in high-latitude sediments (Arney and Wise, 2003; Angori et al., 2007), they are commonly present as high abundance blooms from mid-latitude shelf settings of the Atlantic Coastal Plain (Bybell and Self-Trail, 1995; Weems et al., 2007; Self-Trail, 2011). The similarity of their construction to specimens of the Cretaceous and Tertiary genus *Biscutum*, and their first occurrence immediately following the Cretaceous/Paleogene boundary, suggests that *Hornibrookina* may have evolved from *Biscutum*, a genus long thought to be indicative of higher paleoproductivity (Watkins, 1989). Thus, their increased abundance following the mini-excursion may represent a brief return to both cooler temperatures and increased productivity.

The distribution of some species (*Chiasmolithus bidens, Zygrhablithus bijugatus*, and possibly *Calcidiscus? parvicrucis*) appears to have been controlled strongly by paleoceanographic conditions such as water temperature and paleoproductivity, and these species have abundance patterns that suggest they went into refugium during the PETM event and later repopulated global oceans as paleoceanographic conditions returned to relative normalcy. *Chiastozygus bidens*, a species known to have been partial to cold-water conditions, is present in abundances up to 17% in the Aquia Formation, but is absent from Phase I of the PETM and only reappears in the assemblage once recovery begins. Jiang and Wise (2006) show a similar pattern from Hole 1259B in the tropical Atlantic Ocean, and Wise (pers. comm., 2010) reports this pattern from additional Paleocene/Eocene sections. This suggests that temperatures at SDB during the PETM were greater than during the late Paleocene, and that conditions returned to near normal following the event. The presence of *Chiasmolithus* spp. between 10 and 30% relative abundance at Site 690 (Maud Rise, Weddell Sea; Bralower, 2002) immediately following the CIE suggests that high-latitude sites could have represented cooler water "refugium sites" during Phase I of the PETM.

Z. bijugatus and *Calcidiscus? parvicrucis* also appeared to go into refugium at this time, but possibly for different reasons. *Zygrhablithus bijugatus* is thought by Wei and Wise (1990) and Agnini et al. (2007) to have been controlled by productivity and water depth, thriving in deep-water oligotrophic conditions. In the SDB core, *Z. bijugatus* is present in common to frequent abundances in the pre-PETM Aquia Formation, disappears from the Marlboro Clay and the basal Nanjemoy Formation, which represents the full PETM interval, and then reappears in the NP11 Nanjemoy (Fig. 9). This pattern agrees with the observations of Wei and Wise (1990) and Agnini et al. (2007). High-nutrient influx due to increased continental runoff at this site during the PETM most likely resulted in eutrophic conditions at SDB that were untenable to *Z. bijugatus*. When conditions became more oligotrophic in the early Eocene, *Z. bijugatus* reappeared. *Calcidiscus? parvicrucis* exhibits a similar pattern, suggesting that it may have been responding to the same oceanographic conditions as *Z. bijugatus*. The percent abundance of *Z. bijugatus* at SDB exhibits a very different pattern than exhibited at ODP Site 1209, where it consists of 4.1% average abundance of the nannofossil assemblage throughout the PETM (Gibbs et al., 2006a, 2006b). Open-ocean central gyre locations similar to Site 1209, with deep-water oligotrophic conditions, may represent the "refugium sites" to which *Z. bijugatus*, and possibly *C. parvicrucis*, retreated while unfavorable conditions persisted in shelf environments.

Gibbs et al. (2006a) suggest that *Coronocyclus* and *Neochiastozygus* are mesotrophically to eutrophically adapted opportunists that flourished in the high-productivity setting of the NJ shelf. In the SDB core, the percent abundance of both *C. bramlettei* and *N. junctus* increases dramatically across the CIE (Fig. 6). This pattern is identified from other shelf and slope middle to low latitude localities (Gibbs et al., 2006a; Jiang and Wise, 2006; Bown and Pearson, 2009). The sediments of the SDB corehole reflect a similar paleoenvironment to the Wilson Lake core (NJ), and high productivity is inferred from the increased abundance of the dinoflagellate *Apectodinium* (Willard et al., 2009).

6.5. Excursion taxa and pH

Excursion taxa are identified as those species that first occurred shortly following the onset of the CIE, flourished, and then quickly declined as normal oceanic conditions resumed (i.e., *B. supremus*, *C. bownii*, *D. anartios*, *D. araneus*, *Discoaster falcatus*, *Rhomboaster* spp., and *T. serotinus*); they include the RD assemblage of Kahn and Aubry (2004). Several calcareous nannofossil species most likely represent ecophenotypes that adapted to the extreme conditions present during the PETM by producing coccoliths with irregular spacing of arms (*Rhomboaster* spp.) and malformation of ray tips, lengths, and spacing (*D. anartios* and *D. araneus*). This is the RD assemblage of Kahn and Aubry (2004) which they identify as an indicator of the base of the CIE. However, Angori et al. (2007) report that the RD assemblage occurs slightly higher than the onset of the CIE in expanded Tethyan sections, and this is also recorded at SDB.

Malformation of coccoliths in response to lowered pH values has been documented in modern coccolithophore assemblages (Riebesell et al., 2000; Engel et al., 2005; Langer et al., 2011). However, the response of coccolithophores to changing partial pressure of CO_2 (pCO_2), and thus to changing pH, is not clearly understood. Beaufort et al. (2011) report that decreasing calcification of coccolithophores occurs with increasing pCO_2, and thus with increasing acidity, but that regional variations between coccolith mass and pH can also be a factor. For example, they document a heavily calcified variant of *E. huxleyi* from relatively acidic upwelling waters near Chile. Conversely, Iglesias-Rodriquez et al. (2008) show that high pCO_2 results in increased calcification in a laboratory setting, and show that average coccolith mass has

increased over the past 220 years in response to increased pCO_2. These two results clearly contradict one another, and suggest that the link between pCO_2, pH, and coccolith calcification and malformation is not fully understood.

However poorly understood the links between calcification and pCO_2 are, it is clear that at least a minor percentage of the calcareous nannofossil assemblage during the PETM produced malformed nannoliths, most likely in response to some combination of high pCO_2 and low pH. This phenomenon was documented by Raffi and De Bernardi (2008) from the Walvis Ridge, where they document a cause and effect relationship between discoasterids and environmental change during several hyperthermal events and where they argue it is reasonable to assume that the malformation of the RD assemblage species is a direct correlation to the increased rapid acidification of the ocean during the PETM. This assertion is corroborated in the SDB core, where *D. anartios* and *D. araneus* disappear at 193.9 m, just as initial recovery of $\delta^{13}C$ values begins, and *Rhomboaster* spp. increase in abundance as recovery continues. This pattern suggests that *D. anartios* and *D. araneus* preferred oceanic conditions with lowered pH. The first *Rhomboasters* that appeared at the beginning of the CIE (*R. calcitrapa* and *R. spineus*) with *D. anartios* and *D. araneus*, had long arms. *Rhomboasters* that dominated during the initial recovery (late Phase I) and final recovery (Phase II) were the more blocky "*R. cuspis*" and *R. bramlettei* morphotypes. We interpret this as indicative that the long-armed morphotypes were better adapted to high CO_2 concentrations, and the short-armed morphotypes were better adapted to more normal conditions. Overlap of the two morphotypes in the same samples could result from a preservational overprint on the assemblage or could indicate that both morphotypes could coexist.

Additionally, fluctuations in the abundance of *D. araneus* versus *D. anartios* suggest that differing regional controls influenced the distribution of these taxa, a fact also noted by Raffi and De Bernardi (2008). *Discoaster anartios* is absent from all equatorial to temperate, northern latitude, and southern latitude deep-ocean sites except for Site 1259B, where it was present in only two samples (Jiang and Wise, 2006). Angori et al. (2007) record the presence of very rare specimens of *D.* cf. *D. anartios* at the onset of the CIE at Site 690 (Southern Ocean), stating that the forms found there are very different from those recorded at Tethyan sites. In contrast, *D. anartios* is recorded from all shelf and Tethyan Seaway sections except for Site 549, with abundances equal to or greater than those recorded for *D. araneus*. In SDB, *D. araneus* has its first occurrence before *D. anartios* and is sporadic in abundance throughout the early phase of the PETM, whereas *D. anartios* is present from every sample after its first occurrence. The increase in abundance of *D. anartios* in mid-latitude to Tethyan shelf sections, combined with its absence in deep-ocean settings, suggests that *D. anartios* preferred the mesotrophic to eutrophic conditions associated with many shelf settings.

Included with the excursion taxa, but not considered herein to be ecophenotypes, are *B. supremus*, *C. bownii*, and *T. serotinus*. *Bomolithus supremus* was first identified by Bown and Dunkley Jones (2006) from the Paleocene/Eocene of Tanzania, where it was reported as restricted to Zone NP9. In SDB, this species first occurs at the top of the dissolution zone (202.7 m) and disappears at the unconformable NP10/NP11 boundary. Although it is reported from two mid-latitude shelf sections, it is difficult to say if this species is restricted to these regions. Bown and Pearson (2009) identify the genus *Bomolithus* as being restricted to warm, oligotrophic conditions, but the consistent presence of *B. supremus* throughout the PETM at SDB, where high-nutrient influx from the continent was probable, suggests that this species may have preferred more mesotrophic conditions.

Although, in general, *Toweius* is considered to have preferred cool-water, eutrophic conditions (see Section 6.6 below), one species (*T. serotinus*) appears to have thrived in warm, and possibly eutrophic, conditions. *Toweius serotinus* is a compact form that was first described from Paleocene/Eocene sediments of New Jersey (Bybell and Self-Trail, 1995). This species is restricted to the PETM section of the SDB core, reaching abundances in excess of 30% near the top of the PETM before going extinct. Its abundance increased from <1% at 201 m to over 10% at 199.8 m, just after the first appearance of *D. anartios*. Like other excursion taxa, this species clearly thrived in the warm paleoenvironment of the PETM.

6.6. The genus Toweius

The genus *Toweius* is considered by some to be a generalist with a wide tolerance for both temperature and fertility (Bralower, 2002) and seems to be common in most latitudes. Bown et al. (2004) suggest that *Toweius* spp. was more adapted to cool-water, eutrophic conditions. Percent abundance of this genus has been compared to abundance of the genus *Coccolithus* at almost every PETM site, with varying results. In SDB, *Toweius* spp. average approximately 50% of the total abundance of calcareous nannofossils before and during the early PETM, with decreased abundances recorded only from the dissolution zone at the base of the Marlboro Clay (Figs. 10 and 11). Abundances gradually increase upsection to near 80% at 191.0 m, remaining high until the NP11/NP12 boundary, where they decrease to pre-PETM levels. In comparison, *Coccolithus* spp. decrease slightly across the CIE, but begin to decline to pre-PETM levels as recovery of the system begins (Fig. 10).

Because previous research focused on the genus *Toweius* as a whole, rather than on individual species, confusion exists in its response to oceanographic changes during the PETM. Examination of percent abundance of individual species of *Toweius* shows a clear progression in change of dominance patterns through time (Fig. 11). *Toweius pertusus*, which dominates the assemblage both before and during the PETM, is a generalist with a wide tolerance for both temperature and fertility, as evidenced by the fact that its average percent abundance across the CIE does not change. *Toweius pertusus* begins to decline at the unconformity marked by the Zone NP10/NP11 boundary, and gradually disappears in Zone NP12 in the Nanjemoy Formation. *Toweius eminens* and *T. tovae* are robust species that clearly thrived in the cooler water, mesotrophic paleoceanographic conditions that were present at SDB during the late Paleocene. Their dominance declined in response to changing climate conditions, with *T. tovae* going extinct at roughly the same time as *T. serotinus*, clearly a warm-water form, increased in abundance; *T. eminens* persisted throughout the PETM in low abundances (<1%) and disappeared in the early Eocene.

As conditions returned to normal following the PETM, *T. serotinus* and *T. pertusus* declined in abundance, and *T. callosus* became the dominant species of *Toweius*, reaching its peak relative abundance of 61% at 186.0 m. However, computation of global $\delta^{18}O$ temperatures and $\delta^{13}C$ values (Zachos et al., 2008) clearly shows that although CO_2 decreased following the PETM hyperthermal, global temperatures continued to increase throughout the early Eocene, resulting in the Early Eocene Climatic Optimum (EECO) at approximately 51 Ma and coinciding with deposition of the middle to upper Nanjemoy Formation (NP12–13) sediments. The concomitant rise in abundance of *T. callosus*, followed by the increase in *T. occultatus*, suggests that while these species preferred the return to more mesotrophic conditions that prevailed following the PETM, they were able to tolerate a wide range of temperatures.

7. Conclusions

Detailed analysis of calcareous nannofossil assemblages from the SDB site has provided insight into the biotic response of nannoplankton communities in a shelf setting to extreme global warming. In many respects, assemblages at this middle to outer neritic site responded to the changing climate similarly to assemblages from deeper ocean sites; in some cases, however, calcareous nannofossil assemblages were clearly responding to more regional parameters,

such as nutrient influx, paleodepth, and/or paleolatitude. Based on our analyses, we conclude that:

1. Change in precipitation amounts, resulting in greater erosion of terrestrial sediments and fluvial input into the ocean, occurred at the onset of the PETM at SDB during the early Eocene. This influx, coupled with increased sedimentation rates, resulted in the development of eutrophic conditions in the early Eocene at SDB, although it did not appear to greatly affect salinity at this site.
2. Global extinction of several calcareous nannofossil species is associated with the Paleocene/Eocene boundary at SDB, and is consistent with results previously documented from other sites. A sharp, burrowed disconformity in the SDB core suggests that a minor hiatus is present at this site.
3. Several species indicative of cold-water conditions (*C. bidens*) and/or oligotrophic conditions (*Z. bijugatus*, *C. parvicrucis*) went into refugium during the PETM event and reappeared after a return to more normal oceanographic conditions.
4. Prior to the PETM, a *Hornibrookina* bloom at SDB suggests a return to cooler water conditions following a brief mini-excursion and warming event.
5. With onset of the CIE and concurrent global acidification of seawater, ecophenotypes adapted to low pH and warm-water conditions appeared at SDB and at most other sites. *Discoaster anartios* appears to have preferred high-nutrient shelf settings, while *D. araneus* appears more consistently in more oligotrophic deep-ocean settings, and *Rhomboaster* spp. were cosmopolitan. As recovery began and pH levels increased, *D. anartios* and *D. araneus* went extinct.
6. Opportunists like *C. bramlettei*, *N. junctus* and *B. supremus* flourished in high-productivity shelf environments, only to decline as nutrient levels declined.
7. Different species of *Toweius* are indicators of specific oceanographic conditions, and species-level identification is critical to document paleoceanographic change during the Paleocene and Eocene. *Toweius eminens* and *T. tovae* were dominant during the cooler late Paleocene, preferring mesotrophic conditions. *Toweius serotinus* was largely confined to the PETM interval and appears to have been adapted to warm-water, eutrophic conditions. *Toweius occultatus* and *T. callosus*, which dominated after the extinction of *T. serotinus*, were adapted to warm-water more mesotrophic conditions.
8. Overall low abundances of *Discoaster* spp. and *Fasciculithus* spp. at SDB imply that these dissolution-resistant species, thought to prefer warm, oligotrophic conditions, were more controlled by nutrient availability than temperature.
9. Return to more normal sedimentation and marine conditions during recovery (Phase II) is indicated by the glauconitic shelly muddy sands of the lower Nanjemoy Formation (NP10).

Although changing global climate conditions clearly had a significant influence on calcareous nannofossil assemblages during the PETM, it is also clear that regional controls such as nutrient influx, sedimentation rates, freshwater influx, and paleolatitude also influenced the nannofossil community. As more studies highlight the PETM interval from a range of marine settings, global, regional, and local parameters should become more well-defined, allowing us to predict assemblage response based on setting. This technique can then be applied to other less well-defined hyperthermal events in an effort to determine the manner in which global climate change, nutrient availability, and ocean acidity affect the biotic realm.

8. Taxonomic species list

Bomolithus supremus Bown and Dunkley Jones, 2006
Calcidiscus? parvicrucis Bown, 2005
Calciosolenia aperta (Hay and Mohler, 1967) Bown, 2005
Chiasmolithus bidens (Bramlette & Sullivan, 1961) Hay and Mohler, 1967
Coccolithus bownii Jiang & Wise, 1997
Coronocyclus bramlettei (Hay & Towe, 1962) Bown, 2005
Discoaster anartios Bybell and Self-Trail, 1995
Discoaster araneus Bukry, 1971
Discoaster falcatus Bramlette & Sullivan, 1961
Discoaster multiradiatus Bramlette & Riedel, 1954
Ellipsolithus distichus (Bramlette & Sullivan, 1961) Sullivan, 1964
Hornibrookina arca Bybell and Self-Trail, 1995
Neochiastozygus junctus (Bramlette & Sullivan, 1961) Perch-Nielsen, 1971
Prinsius bisulcus (Stradner, 1963) Hay and Mohler, 1967
Rhomboaster bramlettei (Bronnimann & Stradner, 1960) Bybell and Self-Trail, 1995
Rhomboaster contortus (Stradner, 1958) Bybell and Self-Trail, 1995
Rhomboaster digitalis (Aubry, 1996) Bybell and Self-Trail, 1997
Rhomboaster spineus (Shafik & Stradner, 1971) Perch-Nielsen, 1984
Semihololithus biscayae Perch-Nielsen, 1971
Toweius callosus Perch-Nielsen, 1971
Toweius eminens var. *eminens* (Bramlette & Sullivan, 1961) Bybell and Self-Trail, 1995
Toweius eminens var. *tovae* (Bramlette & Sullivan, 1961) Bybell and Self-Trail, 1995
Toweius occultatus (Locker, 1967) Perch-Nielsen, 1971
Toweius pertusus (Sullivan, 1965) Romein, 1979
Toweius serotinus Bybell and Self-Trail, 1995
Zygodiscus herlyni Sullivan, 1964
Zygodiscus sheldoniae Bown, 2005
Zygrhablithus bijugatus bijugatus (Deflandre *in* Deflandre & Fert, 1954) Deflandre, 1959

Acknowledgments

The authors wish to thank Wilma Aleman Gonzalez, Ellen Seefelt, and Thomas Sheehan (USGS) for sampling the core and Ellen Seefelt for slide preparation. Lively discussions on the PETM with Debra Willard, Thomas Cronin, Laurel Bybell, Lucy Edwards, and Robert Kopp provided insight regarding depositional environments, sediment influx, and biotic response in this region. We wish to thank Debra Willard and Marci Robinson for providing comments on an early draft of this manuscript. This paper benefited greatly from the thoughtful reviews of Timothy J. Bralower and Sherwood W. Wise. This paper is dedicated to the late Dr. Thomas G. Gibson, friend and mentor, whose pioneering work on changing conditions across the Paleocene/Eocene boundary in the Marlboro Clay paved the way for this study. Any use of trade, product, or firm names is for descriptive purposes only and does not imply endorsement by the U.S. Government.

Appendix A. Supplementary Data

Supplementary data to this article can be found online at http://dx.doi.org/10.1016/j.marmicro.2012.05.003.

References

Agnini, C., Fornaciari, E., Rio, D., Tateo, F., Backman, J., Giusberti, L., 2007. Responses of calcareous nannofossil assemblages, mineralogy and geochemistry to the environmental perturbations across the Paleocene/Eocene boundary in the Venetial Pre-Alps. Marine Micropaleontology 63, 19–38.

Angori, E., Monechi, S., 1996. High-resolution calcareous nannofossil biostratigraphy across the Paleocene/Eocene boundary at Caravaca (southern Spain). Israel Journal of Earth Sciences 44, 197–206.

Angori, E., Bernaola, G., Monechi, S., 2007. Calcareous nannofossil assemblages and their response to the Paleocene–Eocene Thermal Maximum even at different latitudes: ODP Site 690 and Tethyan sections. In: Monechi, S., Coccioni, R., Rampino, M.R. (Eds.), Large ecosystem perturbations: causes and consequences: Geological Society of America Special Paper, 424, pp. 69–85.

Arney, J.E., Wise Jr., S.W., 2003. Paleocene–Eocene nannofossil biostratigraphy of ODP Leg 183, Kerguelen Plateau. In: Frey, F.A., Coffin, M.F., Wallace, P.J., Quilty, P.G. (Eds.), Proceedings of the Ocean Drilling Program: Scientific Results, 83, pp. 1–46.

Aubry, M.-P., Ouda, K., 2003. Introduction. In: Ouda, K., Aubry, M.-P. (Eds.), The Upper Paleocene–Lower Eocene of the Upper Nile Valley, Part 1, Stratigraphy: ii–iv.

Beaufort, L., Probert, I., de Garidel-Thoron, T., Bendif, E.M., Ruiz-Pino, D., Metzl, N., Goyet, C., Buchet, N., Coupel, P., Grelaud, M., Rost, B., Rickaby, R.E.M., de Vargas, C., 2011. Sensitivity of coccolithosphores to carbonate chemistry and ocean acidification. Nature 476, 1–17.

Blair, S.A., Watkins, D.K., 2009. High-resolution calcareous nannofossil biostratigraphy for the Coniacian/Santonian stage boundary, Western Interior Basin. Cretaceous Research 30, 367–384.

Bown, P.R., 2005. Palaeogene calcareous nannofossils from the Kilwa and Lindi areas of coastal Tanzania (Tanzania Drilling Project 2003-4). Journal of Nannoplankton Research 27, 21–95.

Bown, P.R., Dunkley Jones, T., 2006. New Palaeogene calcareous nannofossil taxa from coastal Tanzania: Tanzania Drilling Project Sites 11 to 14. Journal of Nannoplankton Research 28, 17–34.

Bown, P., Pearson, P., 2009. Calcareous plankton evolution and the Paleocene/Eocene thermal maximum event: new evidence from Tanzania. Marine Micropaleontology 71, 60–70.

Bown, P.R., Lees, J.A., Young, J.R., 2004. Calcareous nannoplankton evolution and diversity through time. In: Thierstein, H., Young, J.R. (Eds.), Coccolithophores—From Molecular Processes to Global Impact. Springer, New York, NY, pp. 481–508.

Bown, P.R., Dunkley Jones, T., Lees, J.A., Randell, R.D., Mizzi, J.A., Pearson, P.N., Coxall, H.K., Young, J.R., Nicholas, C.J., Karega, A., Singano, J., Wade, B.S., 2008. A Paleogene calcareous microfossil Konservat-Lagerstatte from the Kilwa Group of coastal Tanzania. Geological Society of America Bulletin 120, 3–12.

Bralower, T.J., 2002. Evidence of surface water oligotrophy during the Paleocene–Eocene thermal maximum: nannofossil assemblage data from Ocean Drilling Program Site 690, Maud Rise, Weddell Sea. Paleoceanography 17 (2), 1–11.

Bukry, D., 1973. Low-latitude coccolith biostratigraphic zonation. In: Edgar, N.T., Saunders, J.B. (Eds.), Initial Reports of the Deep Sea Drilling Project, 15, pp. 685–703.

Bybell, L.M., Gibson, T.G., 1994. Paleogene stratigraphy of the Putneys Mill, New Kent County, Virginia, corehole. U.S. Geological Survey Open-File Report 94-217, pp. 1–34.

Bybell, L.M., Self-Trail, J.M., 1995. Evolutionary, biostratigraphic, and taxonomic study of calcareous nannofossils from a continuous Paleocene–Eocene boundary section in New Jersey. U.S. Geological Survey Professional Paper 1554, pp. 1–114.

Bybell, L.M., Self-Trail, J.M., 1997. Late Paleocene and Early Eocene calcareous nannofossils from three boreholes in an onshore-offshore transect from New Jersey to the Atlantic continental shelf. Proceedings of the Ocean Drilling Program, Scientific Results, 150X, 91–110.

Deflandre, G., 1959. Sur les nannofossiles calcaires et leur systematique. Revue de Micropaleontologie 2, 127–152.

Engel, A., Zondervan, I., Aerts, K., Beaufort, L., Benthien, A., Chou, L., Delille, B., Gattuso, J.-P., Harlay, J., Heemann, C., Hoffmann, L., Jacquet, S., Nejstgaard, J., Pizay, M.-D., Rochelle-Newall, E., Schneider, U., Tergrueggen, A., Riebesell, U., 2005. Testing the direct effect of CO2 concentration on a bloom of the coccolithophorid *Emiliania huxleyi* in mesocosm experiments. Limnology and Oceanography 50, 493–507.

Firth, J.V., Wise Jr., S.W., 1992. A preliminary study of the evolution of *Chiasmolithus* in the middle Eocene to Oligocene of Sites 647 and 748. In: Wise Jr., S.W., Schlich, R., et al. (Eds.), Proceedings ocean drilling program: Scientific Results, 120, pp. 493–508.

Frederiksen, N.O., 1979. Paleogene sporomorph biostratigraphy, northeastern Virginia. Palynology 3, 129–167.

Gibbs, S.J., Bralower, T.J., Bown, P.R., Zachos, J., Bybell, L.M., 2006a. Decoupled shelf-ocean phytoplankton productivity responses across the Paleocene–Eocene Thermal Maximum. Geology 34, 233–236.

Gibbs, S.J., Bown, P.R., Sessa, J.A., Bralower, T.J., Wilson, P.A., 2006b. Nannoplankton extinction and origination across the Paleocene–Eocene Thermal Maximum. Science 314, 1770–1773.

Gibson, T.G., Bybell, L.M., 1994a. Sedimentary patterns across the Paleocene–Eocene boundary in the Atlantic and Gulf coastal plains of the United States. Bulletin de la Societe Belge de Geologie 103 (3–4), 237–265.

Gibson, T.G., Bybell, L.M., 1994b. Paleogene stratigraphy of the Solomons Island, Maryland corehole. U.S. Geological Survey Open-File Report 94–708, pp. 1–39.

Gibson, T.G., Andrews, G.W., Bybell, L.M., Frederiksen, N.O., Hansen, T., Hazel, J.E., McLean, D.M., Witmer, R.J., Van Nieuwenhuise, D.S., 1980. Biostratigraphy of the Tertiary strata of the core. Geology of the Oak Grove Core. Virginia Division of Mineralogical Resources, pp. 14–30.

Gibson, T.G., Bybell, L.M., Mason, D.B., 2000. Stratigraphic and climatic implications of clay mineral changes around the Paleocene/Eocene boundary of the northeastern US margin. Sedimentary Geology 134, 65–92.

Hansen, H.J., 1974. Sedimentary facies of the Aquia Formation in the subsurface of the Maryland Coastal Plain. Maryland Geological Survey Report of Investigation, 21, pp. 1–47.

Hay, W.W., Mohler, H.P., 1967. Calcareous nannoplankton from early Tertiary rocks at Pont Labau, France, and Paleocene-Eocene correlations. Journal of Paleontology 41, 1505–1541.

Iglesias-Rodriquez, M.D., Halloran, P.R., Rickaby, R.E.M., Hall, I.R., Colmenero-Hidalgo, E., Gittins, J.R., Green, D.R.H., Tyrrell, T., Gibbs, S.J., von Dassow, P., Rehm, E., Armbrust, E.V., Boessenkool, K.P., 2008. Phytoplankton calcification in a high-CO_2 world. Science 320, 336–340.

Jiang, S., Wise Jr., S.W., 2006. Surface-water chemistry and fertility variations in the tropical Atlantic across the Paleocene/Eocene Thermal Maximum as evidenced by calcareous nannoplankton from ODP Leg 207, Hole 1259B. Revue de Micropaleontologie 49, 227–244.

Kahn, A., Aubry, M.-P., 2004. Provincialism associated with the Paleocene/Eocene thermal maximum: temporal constraint. Marine Micropaleontology 52, 117–131.

Kennett, J.P., Stott, L.D., 1990. Proteus and proto-Oceanus: ancestral Paleogene oceans as revealed from Antarctic stable isotopic results. In: Barker, P.F., Kennett, J.P., et al. (Eds.), Proceedings of the Ocean Drilling Program: Scientific Results, 113, pp. 865–880.

Kennett, J.P., Stott, L.D., 1991. Abrupt deep-sea warming, palaeoceanographic changes and benthic extinctions at the end of the Palaeocene. Nature 353, 225–229.

Kopp, R.E., Raub, T.D., Schumann, D., Vali, H., Smirnov, A.V., Kirschvink, J.L., 2007. Magnetofossil spike during the Paleocene–Eocene thermal maximum: ferromagnetic resonance, rock magnetic, and electron microscopy evidence from Ancora, New Jersey, United States. Paleoceanography 22, PA4103, http://dx.doi.org/10.1029/2007PA001473.

Kopp, R.E., Schumann, D., Raub, T.D., Powars, D.S., Godfrey, L.V., Swanson-Hysell, N.L., Maloof, A.C., Vali, H., 2009. An Appalachian Amazon? Magnetofossil evidence for the development of a tropical river-like system in the mid-Atlantic United States during the Paleocene–Eocene thermal maximum. Paleoceanography 24, 1–17.

Langer, G., Probert, I., Nehrke, G., Ziveri, P., 2011. The morphological response of *Emiliania huxleyi* to seawater carbonate chemistry changes: an inter-strain comparison. Journal of Nannoplankton Research 32, 29–34.

Martini, E., 1971. Standard Tertiary and Quaternary calcareous nannoplankton zonation. In: Farinacci, A. (Ed.), Proceedings of the Second Planktonic Conference, Roma, 1970. Edizioni Tecnoscienza, Rome, 2, pp. 739–785.

McCrea, J.M., 1950. On the isotopic chemistry of carbonates and a paleotemperature scale. Journal of Chemical Physics 18, 849–858.

Mixon, R.B., Powars, D.S., 1984. Folds and faults in the inner Coastal Plain of Virginia and Maryland: their effect on the distribution and thickness of Tertiary rock units and local geomorphic history. In: Frederiksen, N.O., Kraft, K. (Eds.), Cretaceous and Tertiary Stratigraphy, paleontology, and structure, southwestern Maryland and northeastern Virginia. American Association of Stratigraphic Palynologists Field Trip Volume and Guidebook, pp. 112–122.

Mixon, R.B., Powars, D.S., Ward, L.W., Andrews, G.W., 1989. Lithostratigraphy and molluscan and diatom biostratigraphy of the Haynesville cores—Outer Coastal Plain of Virginia, Chapter A. In: Mixon, R.B. (Ed.), Geology and paleontology of the Haynesville cores—Northeastern Virginia Coastal Plain: U.S. Geological Survey Professional Paper, 1489, p. A1-A48.

Monechi, S., Angori, E., von Salis, K., 2000. Calcareous nannofossil turnover around the Paleocene/Eocene transition at Alamedilla (southern Spain). Bulletin de la Societe Geologique de France 171, 477–489.

Muller, R.D., Sdrolias, M., Gaina, C., Steinberger, B., Heine, C., 2008. Long-term sea level fluctuations driven by ocean basin dynamics. Science 319, 1357–1362.

Mutterlose, J., Linnert, C., Norris, R., 2007. Calcareous nannofossils from the Paleocene–Eocene Thermal Maximum of the equatorial Atlantic (ODP Site 1260B): evidence for tropical warming. Marine Micropaleontology 65, 13–31.

Perch-Nielsen, K., 1971. Neue coccolithen aus dem Palaozan von Danemark, der Bucht von Biskaya and dem Eozan der Labrador See. Bulletin of the Geological Society of Denmark 21, 51–66.

Perch-Nielsen, K., 1984. Validation of new combinations. International Nannoplankton Association Newsletter 6, 42–46.

Poag, C.W., 1989. Foraminiferal stratigraphy and paleoenvironments of the Cenozoic strata cored near Haynesville, Virginia. In: Mixon, R.B. (Ed.), Geology and Paleontology of the Haynesville cores—Northeastern Virginia Coastal Plain, Chapter D: Foraminiferal stratigraphy and paleoenvironments of Cenozoic strata cored near Haynesville, Virginia: U.S. Geological Survey Professional Paper, 1489, pp. D1–D20.

Powars, D.S., Bruce, T.S., 1999. The effects of the Chesapeake Bay impact crater on the geological framework and correlation of hydrogeologic units of the Lower York-James Peninsula, Virginia. U.S. Geological Survey Professional Paper 1612, 1–82.

Raffi, I., De Bernardi, B., 2008. Response of calcareous nannofossils to the Paleocene–Eocene Thermal Maximum: observations on composition, preservation and calcification in sediments from ODP Site 1263 (Walvis Ridge-SW Atlantic). Marine Micropaleontology 69, 119–138.

Raffi, I., Backman, J., Palike, H., 2005. Changes in calcareous nannofossil assemblages across the Paleocene/Eocene transition from the paleo-equatorial Pacific Ocean. Palaeogeography, Palaeoclimatology, Palaeoecology 226, 93–126.

Reinhardt, J., Newell, W.L., Mixon, R.B., 1980. Tertiary lithostratigraphy of the core. Geology of the Oak Grove core: Virginia Division of Mineral Resources Publication, 20, pp. 1–13.

Riebesell, U., Zondervan, I., Rost, B., Tortell, P.D., Zeebe, R.E., Mores, F.M.M., 2000. Reduced calcification of marine plankton in response to increased atmospheric CO_2. Nature 407, 364–367.

Rohl, U., Westerhold, T., Bralower, T.J., Zachos, J.C., 2007. On the duration of the Paleocene–Eocene thermal maximum (PETM). Geochemistry, Geophysics, Geosystems 8, Q12002, http://dx.doi.org/10.1029/2007GC001784.

Romein, A.J.T., 1979. Lineages in early Paleogene calcareous nannoplankton. Utrecht Micropalaeontology Bulletin 22, 1–231.

Schmitz, B., Asaro, F., Molina, E., Monechi, S., von Salis, K., Speijer, R., 1997. High-resolution iridium, $\delta^{13}C$, $\delta^{18}O$, foraminiferal and nannofossil profiles across the latest Paleocene benthic foraminiferal extinction event at Zumaya, Spain. Palaeogeography, Palaeoclimatology, Palaeoecology 133, 49–68.

Self-Trail, J.M., 2011. Paleogene calcareous nannofossils of Southern Maryland, South Dover Bridge Core, USA. Journal of Nannoplankton Research 32, 1–28.

Self-Trail, J.M., Willard, D.A., Edwards, L.E., Aleman Gonzalez, W.B., 2010. Terrestrial and marine evidence for climate change across the Paleocene–Eocene boundary: documentation from the South Dover Bridge core, Maryland. Geological Society of America Abstracts with Programs 42, 153.

Sluijs, A., Brinkhuis, H., 2009. A dynamic climate and ecosystem state during the Paleocene–Eocene Thermal Maximum: inferences from dinoflagellate cyst assemblages on the New Jersey Shelf. Biogeosciences 6, 1755–1781.

Sluijs, A., Schouten, S., Pagani, M., Woltering, M., Brinkhuis, H., Sinninghe Damste, J.S., Dickens, G.R., Huber, M., Reichart, G.-J., Stein, R., Matthiessen, J., Lourens, L.J., Pedentchouk, N., Backman, J., Moran, K., the Expedition 302 Scientists, 2006. Subtropical Arctic Ocean temperatures during the Palaeocene/Eocene thermal maximum. Nature 441, 610–613.

Sluijs, A., Bowen, G.J., Brinkhuis, H., Lourens, L.J., Thomas, E., 2007. The Paleocene–Eocene thermal maximum super greenhouse: biotic and geochemical signatures, age models and mechanisms of global change. In: Haywood, W.M., Gregory, F.J., Schmidt, D.N. (Eds.), Deep-time perspectives on climate change: marrying signals from computer modes and biological proxies. The Geological Society of London, pp. 323–349.

Speijer, R.P., Schmitz, B., Luger, P., 2000. Stratigraphy of late Paleocene events in the Middle East: implications for low-to middle-latitude successions and correlations. Geological Society (London) Journal 157, 37–46.

Sullivan, F.R., 1964. Lower Tertiary nannoplankton from the California Coast Ranges. University of California Publications in Geological Sciences 44, 163–227.

Thomas, E., Brinkhuis, H., Huber, M., Rohl, U., 2006. An ocean view of the Early Cenozoic greenhouse world. Oceanography 19, 94–103.

Tremolada, F., Bralower, T.J., 2004. Nannofossil assemblage fluctuations during the Paleocene–Eocene Thermal Maximum at Sites 213 (Indian Ocean) and 401 (North Atlantic Ocean): palaeoceanographic implications. Marine Micropaleontology 52, 107–116.

Van Sickle, W.A., Kominz, M.A., Miller, K.G., Browning, J.V., 2004. Late Cretaceous and Cenozoic sea level estimates: backstripping analysis of borehole data, onshore New Jersey. Basin Research 16, 451–465.

Watkins, D.K., 1989. Nannoplankton productivity fluctuations and rhythmically-bedded pelagic carbonates of the Greenhorn Limestone (Upper Cretaceous). Palaeogeography, Palaeoclimatology, Palaeoecology 74, 75–86.

Weems, R.E., Seefelt, E.L., Wrege, B.M., Self-Trail, J.M., Prowell, D.C., Durand, C., Cobbs III, E.F., McKinney, K.C., 2007. Preliminary physical stratigraphy and geophysical data of the USGS Hope Plantation Core (BE-110), Bertie County, North Carolina. U.S. Geological Survey Open-File Report 2007–1251, 1–163.

Wei, W., Wise Jr., S.W., 1990. Biogeographic gradients of middle Eocene–Oligocene calcareous nannoplankton in the South Atlantic Ocean. Palaeogeography, Palaeoclimatology, Palaeoecology 79, 29–61.

Willard, D.A., Aleman, W.B., Edwards, L.E., Farmer, J., Self-Trail, J.M., 2009. Marine and terrestrial biotic response to climate variability across the Paleocene–Eocene boundary in the mid-Atlantic, USA. Eos Trans. AGU, 90 (52) (PP41A-1492).

Zachos, J.C., Wara, M.W., Bohaty, S., Delaney, M.L., Petrizzo, M.R., Brill, A., Bralower, T.J., Premoli Silva, I., 2003. A transient rise in tropical sea-surface temperature during the Paleocene–Eocene thermal maximum. Science 302, 1551–1554.

Zachos, J.C., Dickens, G.R., Zeebe, R.E., 2008. An early Cenozoic perspective on greenhouse warming and carbon-cycle dynamics. Nature 451 (doi:10.1038).